Carbon 171 (2021) 532–550

Contents lists available at ScienceDirect

Carbon

journal homepage: www.elsevier.com/locate/carbon

A review of surface functionalisation of diamond for thermionic emission applications

Michael C. James [a, b], Fabian Fogarty [a, c], Ramiz Zulkharnay [a], Neil A. Fox [a, d], Paul W. May [a, *]

[a] School of Chemistry, University of Bristol, Cantock's Close, Bristol, BS8 1TS, United Kingdom
[b] Bristol Centre for Functional Nanomaterials, H.H. Wills Physics Laboratory, University of Bristol, Tyndall Avenue, Bristol, BS8 1TL, United Kingdom
[c] EPSRC Centre for Doctoral Training in Diamond Science and Technology, University of Warwick, Coventry, CV4 7AL, United Kingdom
[d] School of Physics, H.H. Wills Physics Laboratory, University of Bristol, Tyndall Avenue, Bristol, BS8 1TL, United Kingdom

ARTICLE INFO

Article history:
Received 1 July 2020
Received in revised form
27 August 2020
Accepted 3 September 2020
Available online 9 September 2020

ABSTRACT

Surface functionalisation of diamond can produce negative electron affinity (NEA), where the conduction band lies higher in energy than the vacuum level. Hydrogen termination is well-known to produce NEA on diamond but can be removed by temperatures above ~700 °C, making it unsuitable for diamond-based thermionic applications, where high temperatures are converted into electricity *via* an electron emission process. In this review article we give an overview of thermionic emission, describe the potential applications of diamond-based thermionic energy converters, then review the different surface termination schemes that can provide a diamond surface with NEA. We discuss the relative merits of the different NEA surfaces that have been developed both computationally and experimentally as alternative cathode materials for thermionic devices.

1. Introduction

A number of advanced technological applications rely for their operation upon controlled electron emission sources. These include emissive flat-panel displays, spacecraft ion engines, high-power microwave amplifiers, X-ray sources, electron microscopy and electron-beam lithography techniques [1–8]. To be emitted from a surface, electrons must possess sufficient energy to overcome the potential barrier situated at the surface-vacuum interface. This potential barrier is known as the work function, ϕ, which is defined as the energy difference between the Fermi level (the electrochemical potential of electrons inside the material) and that of the vacuum level. For semiconductors at normal operating temperatures, the conduction band (CB) is usually empty of electrons while the valence band (VB) is partially or fully occupied. The two bands are separated by an energy band gap of a few eV (*e.g.* 1.1 eV for Si and 5.47 eV for diamond). This means the work function for most metals and semiconductors is also typically several eV. Thus, photons in the UV region of the electromagnetic spectrum or temperatures >1500 K are required to provide sufficient energy to emit electrons at the Fermi energy in the VB directly into the vacuum or to excite them into the CB to be subsequently emitted from there.

For some semiconductors and insulators, however, an alternative emission pathway can occur if the conduction band minimum (CBM) lies higher in energy than the vacuum level. This rare situation is known as negative electron affinity (NEA). In this case, any electrons located in the CB have no emission barrier to overcome to escape the surface. Bulk electrons residing in the VB, or in mid-band-gap states as a result of p- or n-type doping, only need to be excited into the CB for emission to take place. Consequently, materials with NEA are highly desirable for next-generation electron-emission applications.

Fig. 1 shows schematically the difference between positive electron affinity (PEA) and NEA and their relationship to work function. Most semiconducting materials exhibit PEA (Fig. 1(a)), where the Fermi level (E_F) sits midway between the top of the VB and the bottom of the CB. The energy of the vacuum level (E_{vac}) usually sits at an energy higher than the energy of the CBM (E_{CBM}) such that any electrons that become promoted into the CB (by, say, thermal energy or absorption of a photon of the appropriate energy), still have a further energy barrier to overcome in order to

* Corresponding author.
E-mail address: paul.may@bristol.ac.uk (P.W. May).

https://doi.org/10.1016/j.carbon.2020.09.019
0008-6223/

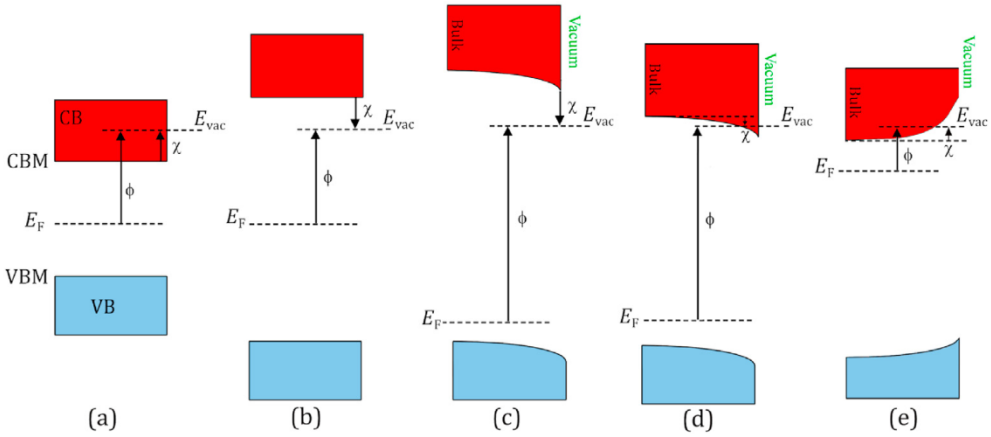

Fig. 1. Schematic diagram illustrating the electron affinity χ and its relationship to work function, ϕ, in relation to a fixed vacuum energy level, E_{vac}, for various semiconductor systems. VB indicates the valence band and VBM its maximum energy, CB indicates the conduction band and CBM is its minimum energy. The position of the Fermi level, E_F, in the band gap varies depending upon whether the semiconductor is p- or n-doped. (a) PEA, (b) true NEA, (c) true NEA in a p-doped material with downward band bending, (d) effective NEA where the downward band-banding pushes the CBM below the vacuum level, and (e) PEA in an n-doped material where upward band banding has pushed the CBM above the vacuum level.

escape the surface and be emitted into the surrounding vacuum. This barrier is the electron affinity (EA), χ (defined as $\chi = E_{vac} - E_{CBM}$) and in this case, is positive. From a non-excited state, the electrons will reside at the Fermi energy and so the total energy required to emit them from the surface, the work function, will be $\phi = \chi + E_F$.

However, in the case of a few unusual materials with large band gaps (such as diamond, cubic boron nitride [9], AlN, AlGaN [10]), the CB has an unusually high energy such that it lies above the vacuum level. In this case the EA is negative, and this situation is known as 'true' NEA (Fig. 1(b)). In this case, any electrons promoted into the CB can be emitted into vacuum with no barrier, and indeed, may emerge with substantial kinetic energies equivalent to the NEA value of a few eV.

This is a rather simplified example. When considering the band structure of a semiconductor, the bands of a material are often depicted as bending up or down at interfaces. This 'band bending' is not a physical effect, but rather a representation of the energy offset due to a charge imbalance at the interface. If the material is p-type doped, the Fermi level is pinned near the VBM, while the CB and VB are pulled downwards at the surface. If the new CBM still remains *above* the vacuum level, then we still have true NEA, as shown in Fig. 1(c). However, if the position of the CB is such that the new CBM induced by band-bending at the surface is now *below* the vacuum level, this leads what is known as 'effective' NEA. Here, any electrons promoted into the CB in the bulk (*e.g.* by heat or photoexcitation), in theory, have enough energy to escape to vacuum. However, as they approach the surface they will either (i) thermalise to the surface CBM and become trapped there by the small surface energy barrier, or (ii) tunnel through the barrier to escape into vacuum. Because electron emission from an effective-NEA surface requires electron tunnelling from the bulk, emission is lower than for a true NEA surface. For n-type semiconductors, the situation is reversed. Now the bands bend upwards and the Fermi level is pinned close to the top of the band gap, near the bulk CBM (Fig. 1(e)). This means the work function can be quite low, however this does not mean that electron emission is facile. Any electrons excited into the bulk CB that do not immediately emit into the vacuum (for example because they are too far from the surface), will start to thermalise to the local CBM. Bulk CB electrons will rapidly end up at the bulk CBM and so face a positive energy barrier (*i.e.* PEA) to escape the surface.

As a result, thermionic emission from semiconductors is a complex process. For ease of electron emission, an *n*-doped material is desirable due to its reduced work function. However, the upward band-banding at the surface induces a PEA which may reduce or prevent electron emission. A *p*-type material may seem undesirable at first due to the need to overcome the large band gap, however if the downward band banding is large and there is also a large NEA, the energies needed to excite and emit electrons may become reasonably small.

2. Thermionic emission

For thermionic emission to occur, a material is heated (typically in vacuum) to a temperature sufficient to allow electrons to be emitted from the surface. Thermionic emission from metals was first studied by Richardson in 1901 [11], and resulted in the Richardson-Dushman equation [12]:

$$J(T) = A_R T^2 \exp\left(-\frac{\phi}{kT}\right) \quad (1)$$

where J is the emission current density, T is the absolute temperature of the emitting material, ϕ is the work function, k is the Boltzmann constant and A_R is known as the Richardson constant. This equation highlights the crucial role in emission played by the work function. For most metals with ϕ ~3–5 eV, the minimum temperature required to obtain usable electron current densities in devices (>1 A cm^{-2}) is typically >1500 °C [13,14], which is hazardous, difficult to attain practically and has high energy requirements. These issues have hindered the development and application of thermionic emission devices for decades. In contrast, for NEA materials, such as diamond, temperatures as low as 800 °C can be used to attain the same current densities, opening the door for a range of practical thermionic devices.

The Richardson constant has been theoretically derived for metals, giving a value of:

$$4\pi mk^2e / h^3 = 120.2 \text{ A cm}^{-2} \text{ K}^{-2} \quad (2)$$

where m and e are the mass and charge of the electron, respectively, and h is the Planck constant. The derivations of Eqs. (1) and (2) assume uniform work function and temperature across the surface, and the model uses a Maxwell-Boltzmann distribution of

electron energies, which is only valid for metals at high temperatures. As a result, the true value of A_R may deviate from the value in Eq. (2), and so often needs be multiplied by an experimentally determined correction factor dependent on the exact nature of the material and surface. Nevertheless, the simplicity of Eq. (2) means it is still widely used for comparison of materials. Table 1 provides a list of common emitter materials and their thermionic emission characteristics, such as melting point, work function, Richardson constant, and emission current densities calculated from these values. Note that due to lack of experimental emission data performed at comparable temperatures, these emission current densities are predicted values based on Eq. (1) using $T = 1500$ K; no account has been made of the stability of the material surface at 1500 K or under electron emission conditions.

Recently, a non-equilibrium Green's function model has been used to consider emission from semiconductor materials such as diamond [15,16]. This model is able to predict properties, such as the Richardson constant, emission onset temperature, and the effect of NEA more accurately than the Richardson model.

3. Thermionic energy converters

Thermionic emission can be utilised for energy generation by employing a thermionic energy converter (TEC). A brief summary of these devices is provided here but more detailed reviews of TECs may be found in Ref. [17,26,27]. As shown by Fig. 2, in a TEC, electrons emitted from a heated cathode (the emitter) travel across a vacuum gap and are captured by a cooler anode (the collector). The difference in work function between anode and cathode creates a potential difference (self-bias) between the electrodes. Connecting the two electrodes allows an electric current to flow from the anode back to the cathode, driving a load. Thus, heat can be converted directly into electricity within a solid-state device that has no moving parts.

For a TEC to work there is usually high or ultrahigh vacuum between the electrodes, otherwise the electrons would likely not reach the collector. The vacuum both increases the collection probability and helps thermally insulate the two electrodes from each other. This insulation is important as it helps to maintain the temperature differential between the electrodes which is essential for maximising the device efficiency.

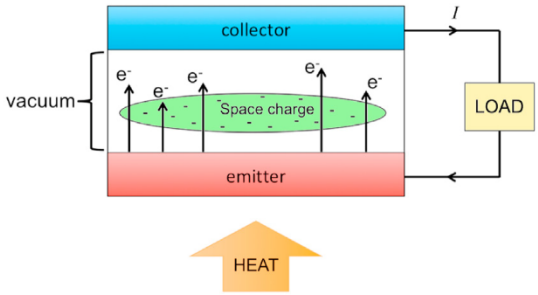

Fig. 2. Simplified schematic diagram of a thermionic emission converter.

3.1. Maximising TEC efficiency

If a TEC is considered to be a simple heat engine, the maximum efficiency is given by the Carnot equation:

$$\eta_{\text{Carnot}} = \frac{T_E}{T_E - T_C} \tag{3}$$

where T_E and T_C are the temperatures of the emitter and collector, respectively. However, a more accurate and realistic method to estimate the maximum efficiency of a TEC is by expressing it as the useful output power divided by the total [28]:

$$\eta = \frac{J_E(V_E - V_C - V_W)}{R + H + J_E(V_E + 2kT_E)} \tag{4}$$

Here, J_E is the emission current density from the emitter, $V_E - V_C$ is the potential difference between the emitter and collector electrodes, V_W is the voltage loss that occurs from connection of the electrodes to a room-temperature load wire, R and H represent heat loss from the emitter through black-body radiation and thermal conduction, respectively, and k is the Boltzmann constant. To ensure a forward bias the collector work function, ϕ_C, must be at least 1 eV lower than that of the emitter, ϕ_E [19]. Also, ϕ_E should be as low as possible to maximise efficiency because the developed bias depends on the difference between the emitter and collector work functions, and if ϕ_E is increased then higher temperatures are required for the same current density (following Eq. (1)). The collector should also be maintained at a low temperature to prevent reverse current generation.

The power density of the device is dependent upon the

Table 1
Properties of some common emitter materials. CNT stands for carbon nanotube. ϕ is the work function, A_R is the Richardson constant, and $J_{1500\ K}$ is the calculated emission current density at 1500 K.

Material	Melting point (K)	ϕ (eV)	A_R (A cm^{-2} K^{-2})	$J_{1500\ K}$ (A cm^{-2})	Ref.
W	3640	4.54	55–104	$6.9 \times 10^{-8} - 1.3 \times 10^{-7}$	[17,18]
Ta	3270	4.10	60	2.3×10^{-6}	[17]
Re	3440	4.70	110	4.0×10^{-8}	[17,18]
Mo	2890	4.15	39	1.0×10^{-6}	[17,18]
Pt	2050	5.40	170	2.7×10^{-10}	[17]
Ni	1730	4.10	60	2.3×10^{-6}	[17]
Ba	1120	2.11	60	11[a]	[17]
Cs on W	-	1.36	3.2	190[b]	[19]
Cs on Si-doped AlGaN	-	2.7–3.2	-	–[b]	[20]
BaO	2196	1.5	0.1	2.1	[18]
LaB_6	2480	2.4–3.4	57–82	$1.1–7.0 \times 10^{-4}$	[21,22]
CeB_6	2825	2.39	19	0.4	[23]
SmB_6	2673	2.76	120	0.14	[24]
h-BN/CNT	-	4.22–4.61	4–1459	$6.0 \times 10^{-8} - 1.1 \times 10^{-6}$	[25]
CNT	3823	2	110–120	47–51	[18]

[a] 1500 K is above the melting point of Ba so no emission would be observed.
[b] It is likely that the Cs layer would have desorbed by $T = 1500$ K.

difference between emitter and collector work functions:

$$P(T) = A_R T_E^2 \exp\left(-\frac{\phi_E}{kT_E}\right)(\phi_E - \phi_C) \quad (5)$$

and the maximum power output occurs at $\phi_E = \phi_C + kT_E$ [29]. This presents a conundrum: as kT_E is relatively small (~0.1 eV), this suggests that the two work functions should be similar for maximum power. But, to maximise efficiency, the difference between emitter and collector work functions should be ≥1 eV. Thus, the different requirements for power and efficiency necessitate a trade-off between the two. Nevertheless, models have predicted efficiencies in excess of 30% to be achievable [28,30] for thermionic devices, making it theoretically comparable or an improvement over other energy generation techniques [30].

3.2. Practical considerations

There are a number of practical considerations when designing a diamond-based TEC. Many of these can be overcome by clever design or good engineering, but some are fundamental to the emission process.

3.2.1. Heating the emitter

First, the emitter needs to be continually heated to maintain electron emission. The emitter is usually heated from the back side, meaning that the emitter and any supports must be efficient thermal conductors to transport the heat through the bulk materials to the emitting surface. Diamond is an excellent thermal conductor, but even though freestanding diamond plates of thickness >3 mm are commercially available, it is unlikely that bulk diamond would be used as the emitter on cost grounds, and due to the limited availability of large area diamond plates. More realistically, the emitter consists of a substrate wafer (Mo metal or Si) onto which a diamond layer a few μm thick is deposited via a chemical vapour deposition (CVD) method. Thus, there are potential heat losses in the substrate bulk and by conduction to its mounts, and at the substrate/diamond interface which can be significant [31]. If the TEC is clamped to a hot surface to provide the heat, as in, for example, an energy-scavenging device, then there will also be losses at the interface between the two. These may be mitigated using high-thermal-conductivity pastes or gels, but these may need replacing frequently and would be limited to the lower end of the usable temperature scale. For solar-power applications, the heat arrives in the form of IR light from the sun, which needs to be collected using a solar-tracking array and focused onto the back of the emitter. Only the IR part of the solar output is required, so the light could be split using prism which directs the IR to the TEC while the rest of the visible and UV light goes elsewhere – perhaps to a conventional photovoltaic cell to maximise usage and efficiency. The IR light that impinges on the back of the emitter needs to be absorbed – any that is reflected reduces the device efficiency. Using a black coating on the surface helps the absorption efficiency. Even better is if the absorbing surface is patterned into micron-sized needle shapes which trap light. These surfaces are known as 'black silicon' or 'black diamond' [32], and can absorb more than 99.9% of the light that strikes them. Whatever absorbing layer is used, there will now be another interface – with its associated thermal barrier – to overcome, before the heat can pass into the bulk. Thus, any efficient emitter will probably have to be comprised of a complex multilayered structure: a black microstructured absorbing layer bonded to a supporting highly conducting bulk layer (diamond, graphite, Si or metal), with an emitting surface layer (diamond) that has been functionalised to give a temperature stable, high NEA surface.

3.2.2. Cooling the collector

In a similar fashion, the collector electrode has to be continually cooled to maintain the temperature difference between the two electrodes. Also, if the collector becomes too hot, it may start to thermionically emit electrons itself – a process called 'reverse emission' – which significantly reduces the device performance. Cooling can be a tricky problem to overcome because there are many mechanisms which heat up the collector. First, the collector is in close proximity to the hot emitter, and will be heated radiatively. It also absorbs 'hot' electrons which collisionally thermalise and dissipate their kinetic energy as heat into the bulk. Any gases present in the gap (see section 3.2.3) may also transport heat from the emitter to the collector via convection.

Water cooling via pipes embedded in the collector is a straightforward method to achieve controllable cooling. However, if the water is *pumped* through the pipes rather than gravity-fed, this requires power, which must be taken into account when calculating the net power generation of the overall TEC.

Further, the collector may not collect all the available electrons. Some emitted electrons may strike and be absorbed by the sidewalls of the device (although this can be avoided by careful design), or instead may reflect/scatter elastically off the collector surface. To reduce this, the collector surface can be patterned or microstructured (in a similar fashion to the back-side of the emitter), in order to efficiently trap electrons and prevent backwards scattering [33].

3.2.3. The vacuum gap and space-charge effects

A high vacuum needs to be maintained between emitter and collector, which must maintain its integrity even when the device is operating at high temperatures (1500 K). This puts a lot of constraints upon the materials from which the housing of a TEC can be fabricated, with stainless steel or a refractory metal, such as Mo, often being used. For a small, sealed system, a thermal getter can be used to maintain the vacuum, however for larger TEC systems continuous pumping is required. Again, the power required to run the vacuum pumps, gauges, and other associated vacuum peripherals, must be factored into the calculations for overall TEC power usage to ensure the power consumed does not exceed the power generated.

A significant problem in TEC devices is space-charge: the accumulation of electrons within the vacuum region. A significant fraction of the thermionically emitted electrons will possess insufficient kinetic energy to travel across the vacuum gap to reach the collector. These slow electrons are then attracted back toward the emitter where they become part of a cloud of electrons that forms a 'virtual cathode' in front of the emitter, greatly suppressing further emission. In terms of energies, repulsion from this virtual cathode creates an additional energy barrier, slightly exceeding that of the vacuum level, that emitted electrons must overcome to reach the collector. Fig. 3 demonstrates the relative energies involved.

There have been various methods reported to minimise space-charge. One approach is addition into the inter-electrode region of low-pressure caesium vapour [28] or gases such as H_2 [34,35] or CH_4 [36]. Cs readily ionises to Cs^+ ions, partially neutralising the negative cloud. H_2 and CH_4 can absorb electrons to form negative ions, and then shuttle these electrons from the emitter to the collector, thereby preventing electrons from lingering near the emitter. Adding H_2 gas to the inter-electrode region was reported to increase emission current while also enabling stable emission at increased temperatures compared with vacuum operation [35]. This improvement was probably due to the renewal of the surface hydrogenation, with new H atoms from the gas continually replacing those lost from the surface by thermal desorption.

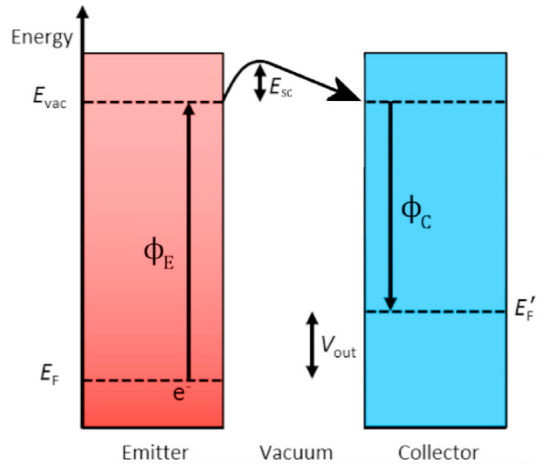

Fig. 3. Energy diagram of a TEC device showing the detrimental effects of space-charge. Electrons in the emitter raised in energy from the Fermi level (E_F) may escape if their energy is greater than the vacuum energy E_{vac}. But there is an additional barrier (E_{SC}) due to the space-charge effect in the inter-electrode region. The work function of the emitter, ϕ_E, must be larger than the work function of the collector, ϕ_C, for a forward voltage to be generated. The voltage generated, V_{out}, is the difference between the Fermi levels in the emitter, E_F and collector, E'_F.

Alternatively, use of a hydrocarbon gas, such as CH_4 [36], is problematic, as the molecules can fragment into carbonaceous residues or polymerise when exposed to high temperatures and electron impacts – either of which will adversely affect the operation of the TEC. Despite the possible performance benefits, adding *any* gas or vapour to the interelectrode spacing has the undesirable effect of increasing heat transport from the emitter to the collector, which may require external power to maintain the electrode temperature difference. For larger systems where the vacuum gap is continuously pumped, any gas additions must be performed continuously, by bleeding tiny flows of the gas into the cell during operation. This comes with the usual increased cost, complexity, and power usage considerations.

Another method to reduce space-charge is to decrease the distance between the two electrodes. The optimal distance is typically a few micrometres [37], which is a compromise between reducing space-charge and minimising radiative heat transfer from the emitter to the collector. An electrode material with NEA, such as diamond, is highly beneficial because the energies of the electron population within the conduction band exceed the vacuum energy, thus minimising the effect of an increased energy barrier from space charge.

Space-charge can also be reduced by applying a small (~10 V) external bias to the TEC cell, to assist in charge extraction at the collector [38]. Similarly, a combination of magnetic and electrical fields on grid or annular ring electrodes placed in the gap has also been used to successfully mitigate space-charge [19,39–41]. Most recently, Bickerton & Fox [42] reported a TEC system incorporating two electric grids which provide opposing electric fields to overcome space charge while minimising power losses. The design creates electron beams within the electrode gap providing a more efficient electron transport from emitter to collector. The problem with all these inter-electrode grid methods is that the complexity of the grids, associated vacuum feedthroughs and power supplies, adds to the cost and decreases the reliability of the overall TEC. Moreover, adding *any* external power supply is not desirable in a device whose purpose is to generate power, not consume it.

Croot *et al.* [43] recently demonstrated that the space-charge effect may be reduced by utilising reverse emission from a β-emitting collector. β-radiation is the emission of high-energy electrons from the radioactive decay of unstable nuclei, such as ^{63}Ni and ^{14}C. Croot *et al.* observed that the peak current from an n-type H-terminated diamond emitter was enhanced by a factor of 2.7 on average when using β-emitting ^{63}Ni as the collector compared with a ^{58}Ni control. This was despite the β-electrons being emitted in the reverse direction (*i.e.* from the collector towards the emitter). It is still unclear why this reduced the space-charge, or whether the improvement in performance was down to other effects. Nevertheless, this is an interesting and unusual development which merits further research.

3.2.4. Emitter surface morphology

There has been little work reported describing the uniformity of thermionic emission across a diamond sample surface, or the effect of local surface morphology upon emission performance. In the case of *field emission*, the applied electric field is concentrated at sharp points or edges on the emitter surface, lowering the effective barrier for electron emission. As a result, most field emission devices are fabricated using microstructured needles [44] or tips (*e.g.* Spindt tips [45]) and the electrons are emitted from the top of these tips. However, in the case of field emission from diamond, there is evidence that the presence of nanoscale graphitic inclusions on the surface of the polycrystalline CVD diamond films is more important than edges or tips. The nanoscale sp^2-carbon inclusions situated in grain boundaries locally lower the barrier for emission. Thus, field emission is believed to originate mainly from the grain boundaries surrounding crystallites rather than from the top of the grains [46,47].

In contrast, the mechanism for thermionic emission from diamond is less well understood. Robinson *et al.* [48] used a hemispherical energy analyser to measure thermionic electron-energy distributions from boron-doped diamond emitters at elevated temperatures. The results showed that emission occurred at different points on the surface from regions with differing work functions. The relative peak intensities, representing each work function, changed with temperature indicating instability in the emitter surface chemistry. At higher temperatures, a residual gas analyser attached to the chamber suggested that hydrogen adsorbates were desorbing from the diamond surface, creating patches of hydrogenated and bare diamond surface.

Using a similar set-up, Uppireddi *et al.* [49] measured the thermionic electron emission distribution from nanocrystalline diamond (NCD) films from 700 to 900 °C, and the data were fitted to a free-electron-theory model. The films had a consistent effective work function of 3.3 eV, but also exhibited some emission peaks corresponding to higher work functions, which the authors suggested were related to instabilities in the NCD surface chemistry.

Experiments using energy-filtered photoemission electron microscopy (EF-PEEM) were used to measure the work function of AlO-terminated diamond surfaces as a function of annealing temperature [50]. As shown in Fig. 4, the work functions are relatively uniform across the sampled area, although the emission is rather patchy. This shows that non-uniformity in the AlO coverage, together with slight imperfections and scratches on the surface, can significantly affect the electron emission. These results seem to suggest that thermionic emission is an extended surface phenomenon, and not localised to particular surface structures, such as edges, tips or grain boundaries. However, much more work needs to be done to identify the nature of the thermionic emission sites and to understand the emission mechanism with relation to local morphology.

3.2.5. TEC applications

Despite the various practical problems outlined above, TECs still promise a route to produce power efficiently, continuously, and

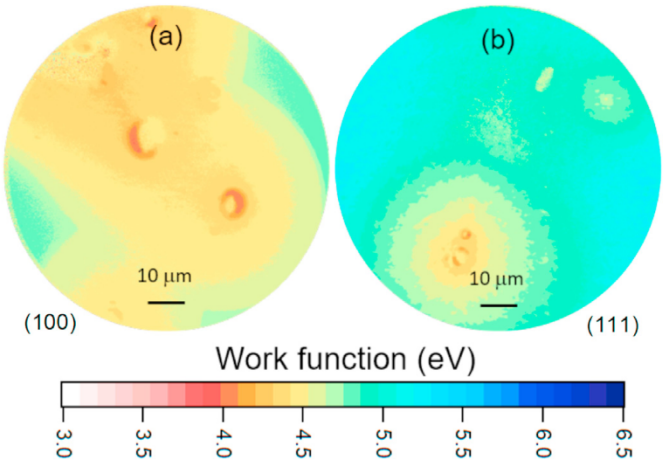

Fig. 4. EF-PEEM images showing the work function measured from (100) and (111) diamond terminated with AlO. The emission is broadly uniform, although there are patchy areas due to incomplete coverage by AlO. Taken from Ref. [50] with permission.

reliably, in a compact solid-state device with no moving parts. Not surprisingly, one of the most successful applications of TECs to date is for powering spacecraft. The Soviet Union used TECs to generate power as part of the 5 kW TOPAZ nuclear reactors, which were used for two missions in 1987 [26]. More recently, use of TECs have been considered for missions to the Sun and Mercury [51]. By concentrating solar heat using a sun-tracking parabolic reflector, TECs could be an alternative for renewable energy generation terrestrially [27,36,52,53]. Alternatively, TECs could be combined with existing combustion-heated systems for domestic electric-power co-generation, and waste-heat scavenging [54,55]. Small, portable TEC devices have also been suggested as method of reducing the heat signature of military vehicles, making them harder to detect by IR thermometry or target with heat-seeking weapons.

3.2.6. TEC enhancements and variants

The efficiency of a basic TEC device can be improved by using either light or additional electrons to enhance the electron emission process. In the first approach - photon-enhanced thermionic emission (PETE) - photon absorption and thermal energy both contribute towards energising electrons into the conduction band. As shown in Fig. 5, in the cathode (emitter), photons with energy greater than the band gap excite electrons from the VB into the CB creating a photon-enhanced population. Simultaneously, the heated substrate thermally excites electrons from the Fermi level to the CB, creating a corresponding thermal population. These two populations combine and thermalise at the emitter surface. The highest-energy electrons are now above the vacuum level, so are thermionically emitted.

Elfimchev *et al.* [56] studied this photon-enhancement effect and reported that electron emission increased by several orders of magnitude at lower temperatures, but had a smaller enhancement effect at thermionic temperatures. Despite the improved emission efficiency, PETE devices generally require that the sunlight strikes the front of the emitter rather than the back side. Thus, they need to be designed with a UV-transparent window into the vacuum cell, and with unrestricted line-of-sight from the window to the emitter surface, adding significantly to the complexity and cost. A solution to this was proposed by Sun and co-workers [57], which consisted of a PETE structure where the emitter surface was directly illuminated through a transparent collector. They also examined the individual contributions of photo- and thermionic emission, and the effects of the interface and interlayer conditions [58,96].

For solar applications involving PETE, the large band gap of diamond (5.47 eV or 225 nm) means it is transparent to solar radiation. To solve this, Bellucci *et al.* [59] proposed an electrode structure using a blue/black p-type diamond layer on an intrinsic diamond substrate as the absorption layer, and a hydrogen-terminated diamond layer on the emission surface. In subsequent papers, they discussed the fabrication of a nanotextured diamond surface [60,61] to enhance solar absorption. They have also proposed forming graphitic microchannels to improve conductivity through the diamond layer [62], as shown in Fig. 6.

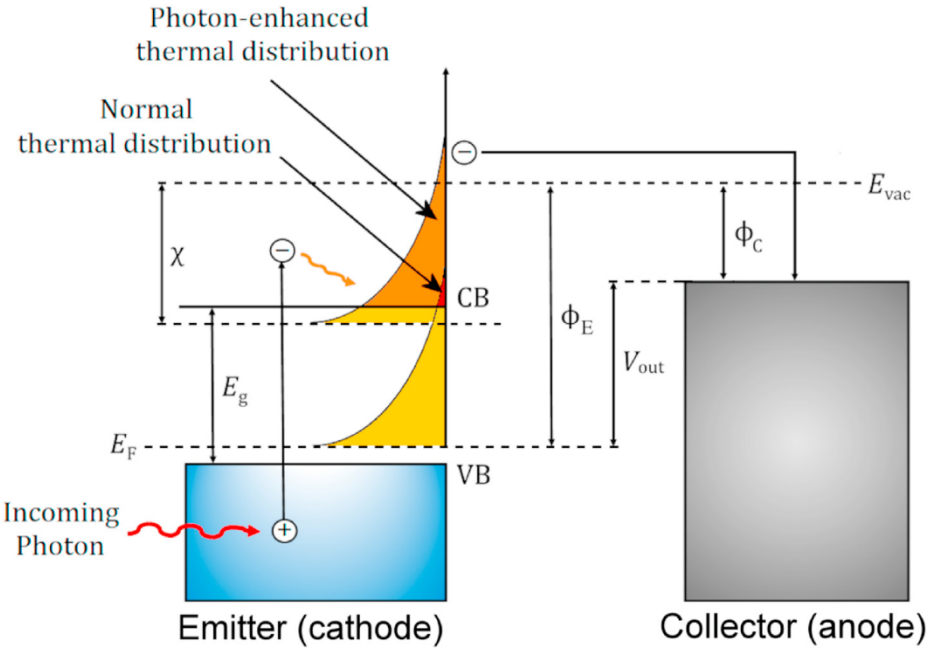

Fig. 5. Schematic energy diagram for PETE.

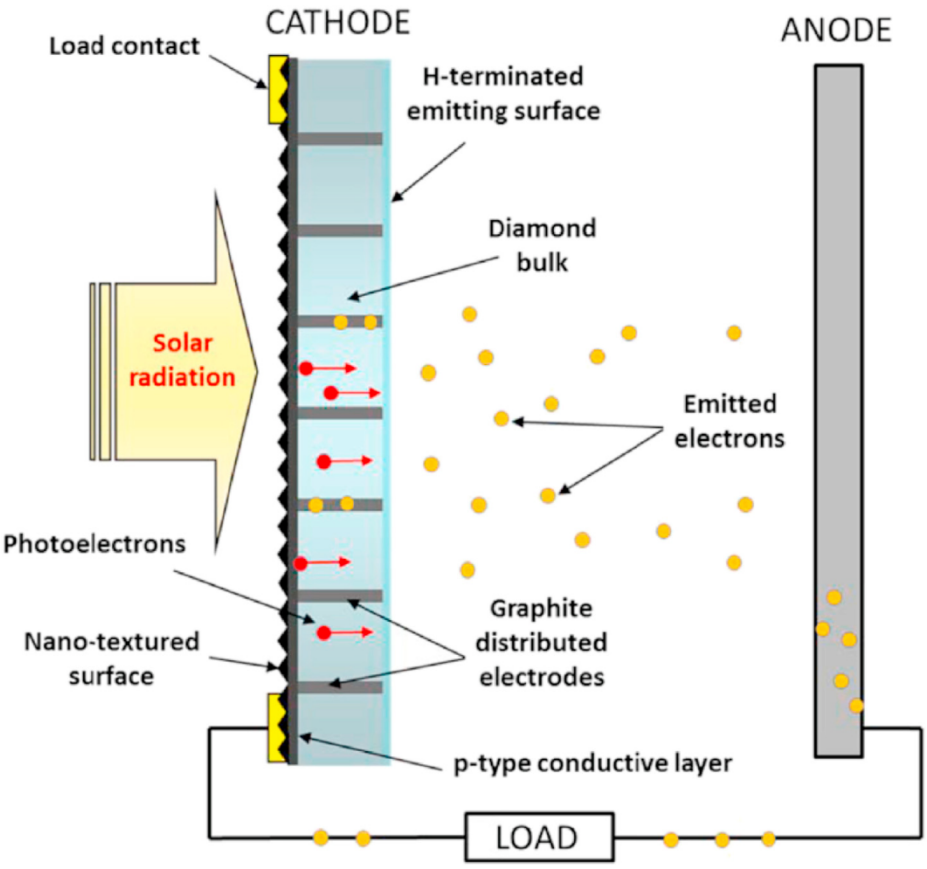

Fig. 6. Diamond-based PETE device concept. The absorption layer surface is nanotextured to enhance the solar absorption and consists of p-type diamond. The emitting surface is H-terminated. A number of graphitic microchannels are fabricated to enhance conductivity through the material. Reprinted with permission from Refs. [62]. Copyright Elsevier (2016).

The higher efficiencies make PETE an interesting new area of research for thermionic materials. While a number of semiconductor materials have been studied for PETE devices, diamond is well placed for use in this technology due to its NEA surface and because it does not suffer from thermal instability at higher temperatures unlike III-V semiconductors. However, the added cost and complexity may prove too much of a barrier for PETE devices to be commercially viable.

Another variant on the basic TEC design involves using electrons from radioactive β−decay to assist the thermionic process. This approach differs from the report by Croot *et al.* mentioned earlier [43] who used a β-source as the collector, in that, in this case, the β-source is now the emitter. The idea is that ^{14}C (obtained from waste radioactive graphite previously used in nuclear power stations) is burnt in hydrogen to produce $^{14}CH_4$. This gas is then fed into a conventional CVD reactor which deposits a layer a few microns thick of isotopically pure ^{14}C diamond onto a TEC emitter (made from metal or doped standard diamond). Being a β-emitter, the layer of ^{14}C continuously emits a stream of electrons with a half-life of ~6000 years. When used as the heated emitter in a TEC, the β electrons and thermionically emitted electrons should combine to increase the net current flowing and hence the power and efficiency of the device. Few experimental results have yet been reported, but a number of research groups are actively researching this area.

Variations on this concept which use only the β-layer without thermionic enhancement are often referred to as a 'nuclear battery' or 'betavoltaic battery' [63]. Other designs based on layers of alternating p- or n-doped diamond sandwiched between ^{14}C diamond emitting layers [64], or that utilise ^{63}Ni or tritium as the radioactive sources [65], have also been proposed. Such devices would produce electrical power almost indefinitely (thousands of years), and can be made into small, portable, sealed solid-state packages, with no moving parts and which require zero maintenance. The output power per device would be tiny, maybe only a few μW, but hundreds or thousands of devices could be joined together in series to produce higher powers, if required. Because the battery is always on, it could continuously trickle-charge a capacitor ready for intermittent high-power use, *e.g.* a burst transmitter on a spacecraft. Other suggested uses include areas where replacing a dead battery is difficult, costly or impossible, such as military applications (*e.g.* remote surveillance), aerospace applications (*e.g.* sensors inside jet engines) or medical applications (perpetual pacemakers). There are numerous commercial applications, such as for domestic use (watches, calculators, mobile phone chargers, *etc.*), and powering 'smart' devices for the 'Internet of Things' [66].

4. Diamond

Diamond is a wide-band-gap semiconductor ($E_g = 5.47$ eV) with many favourable properties including hardness, chemical stability and high carrier mobilities [67]. Diamond films can be grown by CVD methods or as particles or gemstones by high-pressure high-temperature (HPHT) methods. Diamond films may be doped *p*-type by introduction of boron impurities [68], or *n*-type by introduction

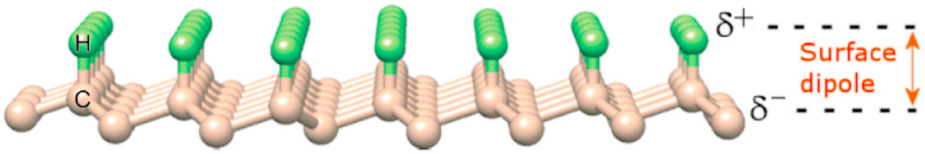

Fig. 7. Schematic diagram of the surface dipole on a hydrogen-terminated (111) diamond surface.

of nitrogen [69] or phosphorus [70] impurities. Boron acceptor states are located 0.37 eV above the VBM, while nitrogen and phosphorus donor states are located 1.7 eV and 0.67 eV below the CBM, respectively [71]. As well as changing the electrical conductivity of the bulk, these dopants also produce band bending at the surface, and this can have a significant effect upon the magnitude and sign of the electron affinity. Larsson [72] used DFT methods to calculate the EAs for a range of terminating species (H, O, OH, NH_2, F) on undoped, *p*-doped, and *n*-doped diamond (100) and (111) surfaces. She found the EA values depended significantly upon all these factors: adsorbate, adsorbate geometry (*e.g.* linear or bridging), diamond surface orientation, and, importantly, bulk doping type. Thus, care must be exercised when using reported experimental or theoretical EA values, especially when comparing values, to ensure that these factors are known in each case. This problem often arises when measuring EA values using surface analysis characterisation methods, such as X-ray photoelectron spectroscopy (XPS), which require an electrically conducting surface to function. For undoped diamond, this problem is often solved by depositing a thin, B-doped diamond layer (with near-metallic-conductivity) onto the diamond surface, which can then be chemically functionalised, as required. But any XPS measurements of EA from this surface will relate to the B-doped diamond layer, not the intrinsic diamond bulk, making direct comparisons with theory problematic.

Diamond is a highly promising material for electron emission devices because, in addition to its well-known list of superlative bulk properties [67], diamond can possess an NEA surface if it is terminated with a suitable chemical species. The most common species found on the surface of natural diamond and CVD diamond films is hydrogen (see section 4.1). The small difference in electronegativity between carbon and hydrogen creates a surface dipole, where the positive charge is outermost, as shown in Fig. 7. Thus, electrons are, to some extent, repelled from the negative bulk and attracted toward the positive H layer and then emitted out of the surface, with a reduced barrier for emission. This can lead to an NEA surface if the H coverage is sufficiently high. The hydrogenated surface can be further functionalised relatively easily by modifying the C–H bonds using a variety of standard wet chemistry and plasma techniques [73], to produce new NEA surfaces with improved emission behaviour and thermal stability, as discussed later.

Electron emission from diamond has been demonstrated using different excitation sources, such as from photon absorption (photoemission [74]), particle impact (secondary electron emission [75]), thermal energy (thermionic emission [38]) and application of an electric field (field emission [46]). Although the material requirements for these applications (stable NEA surface, low work-function, *etc.*) are similar, in this review we shall focus upon thermionic emission.

4.1. Hydrogen termination

Hydrogen-terminated diamond possesses an NEA measured as −1.3 eV for the (100) surface and −1.27 eV for the (111) surface [76,77]. CVD diamond is deposited in a hydrogen-rich atmosphere and so the as-grown surface is automatically H-terminated. For diamond with other types of termination or a bare surface that has lost its terminating groups, heating in a hydrogen gas atmosphere or H_2 plasma treatment recreates the H termination and allows easy and reproducible NEA surfaces to be formed [78].

The CVD diamond growth conditions can be controlled to favour different growth surfaces - usually the (100), or less commonly, the (111) surfaces. These H-terminated diamond surfaces have been widely studied computationally with density functional theory (DFT), and their structures verified experimentally [79]. As shown in Fig. 8, hydrogen atoms bond to each surface sp^3 carbon to satisfy its four-fold valency. For the (111) surface this produces rows of single H atoms pointing normal to the surface (Fig. 8(a)), but for the (100) surface, addition of two H atoms in their usual positions on adjacent surface carbons would lead to partial overlap of the H's; thus, on energetic grounds the surface reconstructs into (2 × 1) dimer rows (Fig. 8(b)).

Table 2 gives the values of two key parameters - adsorption

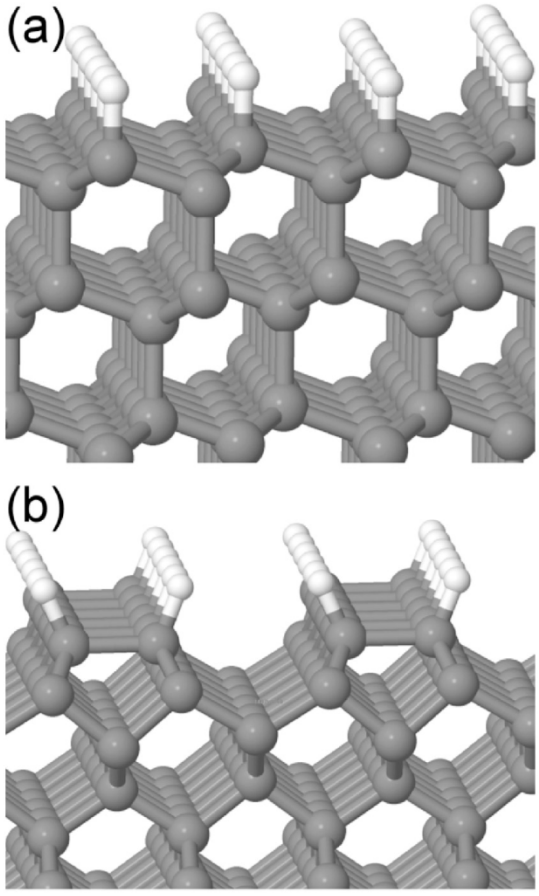

Fig. 8. Simulations of the (a) (111) and (b) (100) H-terminated diamond surfaces, respectively. Carbon is grey and hydrogen white.

Table 2
Theoretical studies of adsorption energies along with corresponding electron affinity (EA) of adsorbates on the bare diamond surface. ML = monolayer.

Termination	Surface	Coverage (ML)	E_{ad} (eV/atom)	EA (eV)	Ref.
H	(100)	1	−4.14 – −5.36	−1.94 – −2.2	[88–93]
H	(111)	1	−4.37	−1.98	[94]

energy and electron affinity - calculated for both H-terminated surfaces. The NEA values of ~ −2 eV are sufficient for reasonable thermionic emission; threshold temperatures are typically between 300 and 600 °C while maximum emission-current density is typically in the range of $10^{-4} - 10^{-3}$ A cm^{-2} [30,38,53,80–84].

The adsorption energy, E_{ad}, is an indication of the strength of the C–H bond; it determines the temperature stability of the surface. E_{ad} is defined as the energy of a surface plus adsorbate(s) relative to their respective energies when isolated from each other. The isolated surface will be in a stable form *e.g.* dimer rows or Pandey chains for bare (100) and (111) surfaces, respectively, or the ether oxygenated surface for addition to (100) O-terminated diamond. Following standard convention, a negative E_{ad} means the adsorption process is exothermic. The magnitude of E_{ad} gives an indication of how likely the adsorbate is to stick to diamond, and its subsequent stability on the surface. The more negative the adsorption energy, the more strongly the adsorbate is attached to the surface and the higher the temperatures required for it to thermally desorb.

For H on diamond, the relatively low value of adsorption energy of ~ −4 eV means that these surfaces are only stable to around 600-800 °C – after which the H atoms begin to desorb leaving a bare surface with a PEA and a corresponding decrease in the emission current. As shown in Fig. 9, even cycling the temperature to 600 °C will cause a decrease in the maximum emission current and an increase in the emission onset over time [43]. The hydrogenated surface also oxidises in air or water over a period of hours or days, and can undergo surface transfer doping with airborne adsorbates [85], all of which result in loss of the NEA. It is therefore of interest to find a suitable diamond surface termination that exhibits similar NEA properties to hydrogen-terminated diamond but with greater stability under ambient conditions and/or at higher temperatures in vacuum [53,83,86,87].

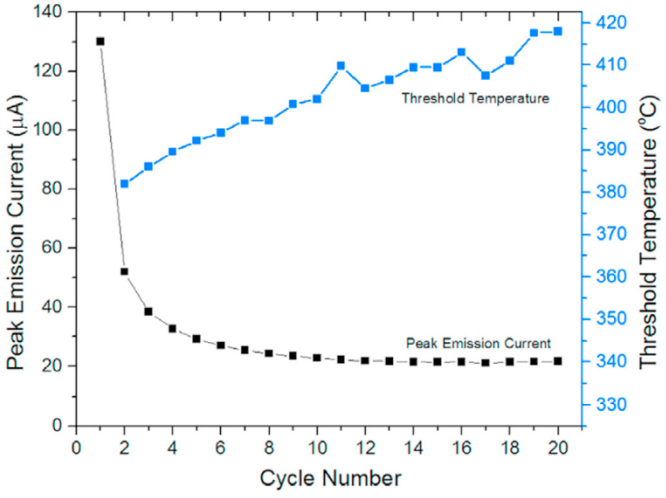

Fig. 9. Thermal cycling of a H-terminated diamond cathode up to 600 °C shows the peak emission current decreases and the threshold temperature for emission increases with an increasing number of emission cycles. Adapted from Ref. [43] under the CC BY licence.

4.2. Thermionic emission from diamond

There have been a number of thermionic emission experiments performed using H-terminated diamond. A summary of this experimental work is provided in Table 3. The diamond is often doped to improve conductivity; in particular, n-type doping is desirable for thermionic emission as it raises the Fermi level (recall Fig. 1(e)). Despite nitrogen having a deep donor position of 1.7 eV, this is not such a problem at the elevated temperatures used for thermionic devices. Thermionic experiments performed using N-doped H-terminated diamond have reported Richardson constants in the region 68–70 A cm^{-2} K^{-2} with associated work function values of 1.99 eV [82] and 2.88 eV [30]. Nitrogen-doped diamond typically achieves current densities of 1–5 mA cm^{-2} at temperatures between 500 and 700 °C [38,52,82]. Ultrananocrystalline N-doped diamond samples have shown particularly low work functions of 1.29–1.67 eV but have small values of the Richardson constant of between 0.69 and 3.67 A cm^{-2} K^{-2} [34,81,84].

Phosphorus-doped diamond has shown a lower work function than nitrogen-doped diamond at 0.9 eV for polycrystalline diamond [29] and 0.67 eV for (100) single-crystal diamond [30]. However, the associated Richardson constants were low, measured as 10^{-5} A cm^{-2} K^{-2} and 10^{-7} A cm^{-2} K^{-2}, respectively. This meant the samples had relatively low emission currents, which was believed to be due to high resistivity and low mobility as a result of the low P doping concentrations of ~10^{18} cm^{-3}. A higher Richardson constant of 15 A cm^{-2} K^{-2} was observed with a doping level 5×10^{20} cm^{-3}, achieving an emission current density of 8 mA cm^{-2} at 600 °C [95].

Because the diamond is grown up to a few microns thick upon a substrate, the material properties of the substrate and the interface region also play a part in the emission process [96]. A comparison of different substrates showed that CVD diamond deposited heteroepitaxially onto rhenium substrates had larger values for the Richardson constant and current density than diamond deposited on either molybdenum or tungsten substrates. This was attributed to the fact that during CVD, Mo and W form thin carbide layers between the metal and diamond. Although only a few nm thick, this electrically resistive carbide layer impedes the flow of electrons from the back contact to the diamond surface. In contrast, Re does not form a carbide, and so electron transport is unimpaired [80].

Other factors which may affect the emission properties arise from the varied surface morphology of diamond, which can have different crystallite sizes, morphologies, and be patterned into a variety of nanostructures. Unfortunately, very little has been reported in the literature about the effect of surface morphology upon thermionic emission. Regarding crystal size, ultrananocrystalline diamond (UNCD) or polycrystalline diamond is formed from heteroepitaxial CVD. The inclusion of grain boundaries generally assists with emission by improving electron transport to the surface. Indeed, for field emission it is now believed that the electron emission originates from grain boundaries at the surface which lower the local effective barrier to emission in the presence of an electric field [46,47]. However, thermionic emission does not utilise a significant applied field, and so this mechanism will not apply. The nature of the emission site(s) in thermionic emission, therefore, remain unproven, and suggests excellent

Table 3
Different studies of electron emission properties using a H-terminated diamond cathode. UNCD = ultrananocrystalline diamond, ϕ = work function, A_R = Richardson constant, and $J_{1500\ K}$ is the calculated emission current at 1500 K.

Dopant	Crystal	Substrate	Concentration (cm^{-3})	ϕ (eV)	A_R (A cm^{-2} K^{-2})	$J_{1500\ K}$ (A cm^{-2})	Ref.
N	UNCD	Mo	~10^{21}	1.29	0.84	88	[84]
N	UNCD	metallic	-	1.67	1.33	7.3	[34]
N	UNCD	Mo	-	1.42	0.69	26	[80]
N	UNCD	W	-	1.39	1.19	57	[80]
N	UNCD	Mo/Re	-	1.40	3.67	160	[80]
N	Polycrystal	Mo	-	2.22	5.96	0.47	[86]
N	Polycrystal	Mo	4×10^{19}	1.5–1.9	0.1–10	0.093–210	[38]
N	Polycrystal	*n*-type Si	2.4×10^{20}	1.99	70	32	[82]
N	(100)	diamond	3.3×10^{19}	2.88	68	0.032	[30]
N	(100)	diamond	4×10^{19}	2.4	-	-	[52]
P	Polycrystal	metallic	~10^{18}	0.9	1.0×10^{-5}	0.021	[53]
P	Polycrystal	Mo	5×10^{20}	2.3	15	0.63	[95]
P	(100)	diamond	~10^{17}	0.67	2.3×10^{-7}	0.0029	[30]
P	(100)	diamond	~10^{18}	0.84	-	-	[30]
P	(111)	diamond	4.4×10^{18}	1.45	0.011	0.33	[30]

possibilities for further research. The same is true of micro- or nanoscale surface structuring, such as fabrication of tips or needles. These are known to improve field emission currents, again due to the enhancement of the applied field at sharp tips or edges – but the effects of geometry upon thermionic emission from diamond surfaces has yet to be studied in detail. However, we can predict that the larger surface areas available in patterned films are likely to increase the emission current compared to that from smooth surfaces.

When compared to other thermionic materials in Table 1, it can clearly be seen that diamond is a highly promising material for thermionic applications, with the potential for exhibiting emission currents as high as 210 A cm^{-2} at 1500 K making it comparable to carbon nanotubes or to Cs on W, while outperforming conventional emitter materials such as LaB_6 and CeB_6 by several orders of magnitude.

4.3. Alternative surface terminations

Among the multiple factors which influence the electron affinity of a diamond surface, the physical and chemical properties of any adsorbates are often key. The process of replacing one or more terminating H atoms with other atoms or bulky groups, perhaps with very different chemical properties to that of the diamond bulk, often results in surface reconstruction which can aid or hinder thermionic electron emission. Moreover, these surface modifications can vary with time, either by desorption of surface species, loss of dopants via in diffusion, or gradual relaxation of the surface into a different structure. Such thermionic 'aging processes' have been studied on barium-impregnated tungsten cathodes [97], but very little work has been done on diamond. A recent report by Dominguez-Andrade *et al.* [98] is one of the few papers to investigate the interplay between thermionic emission and temperature-driven dynamic surface transformation processes. To model thermionic emission, they used a modified Richardson-Dushman equation which included new terms for the extent of adsorbate coverage on the surface linked to variable work function values for different surface features. The model successfully reproduced the thermionic emission behaviour of H-terminated diamond surfaces, replicating the effect of dynamic changes in surface phases due to successive thermal desorption of the H from different surface sites. For the case of hydrogenated (100) single-crystal diamond, the model allowed the authors to identify the fully terminated dimers of the C (100)-(2 × 1):H surface reconstruction on flat terraces - the most thermally stable form of H on that surface - as the origin of the majority of the emission. The model also worked for thermionic emission from the more complicated surfaces of polycrystalline diamond films.

Although these adsorbate-induced changes to the surface structure are the true key to understanding electron emission, these are very difficult to study without the use of surface science techniques with atomic-level resolution or advanced computer modelling. A rather simple but nonetheless useful approach, however, is to compare the difference in electronegativity (EN) between the carbon atoms in the bulk diamond (Pauling EN = 2.6) and that of the adsorbate forming the outermost layer. If the terminating atom is more electropositive than C, for example H, a surface dipole will be created with the outermost layer being slightly positively charged. Such surfaces tend to exhibit NEA. Conversely, surface atoms which are more electronegative than C (*e.g.* N, O, S, and all the halogens) create a dipole with the outermost layer being slightly negatively charged. In this case, the surface usually has a PEA because the negative outer surface makes it more difficult to extract electrons from the bulk. As a generalisation, the larger the difference in EN, the greater the NEA or PEA values. Pauling EN values for selected elements are given in Fig. 10. Elements with EN < 2.6 include all metals, especially those in Group I and II, in addition to some metalloids and non-metals. Therefore, there is considerable scope for finding an alternative to H-termination for use in thermionic devices. It should, however, be noted that many of these elements will not adsorb or react with a diamond surface, and even if they do, they may subsequently oxidise or delaminate.

For surface terminations involving molecular groups such as amine (NH_2) or hydroxyl (OH) groups, the value and sign of the net dipole is often not so obvious, but can be calculated using *ab initio* methods [100]. For more complex terminations such as these, there may be sequential layers of opposite charges present near the surface; whether the surface ultimately ends up as overall PEA or NEA depends on the nature of the bonding and the structure of the adsorbed layer (see section 4.3.7).

In natural diamond or diamond produced by high-pressure high-temperature or CVD techniques, the surface carbon atoms are usually terminated with monovalent species such as H or OH, or multivalent species such as O or N that bond to multiple carbons. All such terminating species attach to one or more carbon atoms using conventional covalent (sigma) bonds, which behave identically to covalent bonds in other molecules. Standard chemical procedures or plasma treatments can break these bonds and replace the surface adsorbates with new ones tailored for a particular application. Depending on its chemical nature and physical structure, the new adsorbate may attach to the diamond

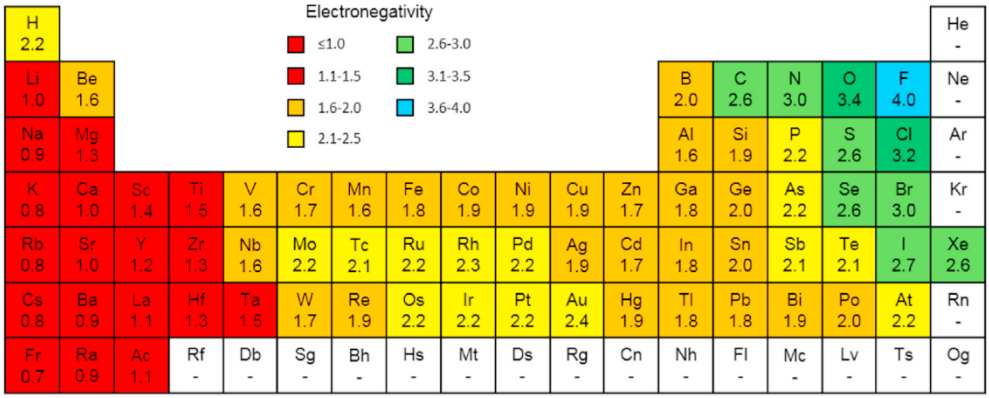

Fig. 10. Periodic Table of the elements and their respective Pauling electronegativity values [99]. An NEA surface on diamond requires surface groups with EN < 2.6, while PEA requires EN > 2.6.

surface in a variety of ways, including conventional sigma bonds, covalent bonds with substantial ionic character, or metal-carbon multi-centre bonds. We now discuss several such surface termination strategies that have been reported to produce an NEA surface suitable for thermionic emission.

4.3.1. Metal terminations

The most straightforward method to produce an NEA surface on diamond is to deposit an element (usually a metal with EN < 2.6) directly onto the bare diamond surface. This can be achieved in ultra-high vacuum (UHV) by first heating the diamond to remove the existing surface termination and then using techniques such as evaporation, sputtering or atomic layer deposition (ALD), to deposit the metal. The sample is usually then annealed at high temperature in vacuum to make the metal react with and bond directly to the carbon. Monolayer or sub-monolayer coverage is preferential since thicker layers result in bulk adsorbate characteristics affecting electronic structure at the surface.

Relatively few metal adsorbates have been studied experimentally to date, but several of those that have show promising thermionic characteristics. Nemanich and co-workers demonstrated that thin (<10 Å) layers of Co, Cu and Zr on diamond exhibit small NEA values, measured between −0.15 eV and −0.70 eV [101–103]. Ni on (100) and both Ti and Ni on (111) diamond also exhibit NEA [104,105]. Thermionic emission from a 3 Å Ti layer on N-doped diamond gave a ~2 × increase in emission current relative to a comparable H-terminated diamond sample. This was due to the greater thermal stability of the surface allowing a temperature of 950 °C to be reached [106] without the surface layer desorbing. A similar result was found with Zr-terminated diamond [107].

By contrast, a wider variety of metals have been studied theoretically; a summary of calculated adsorption energies and electron affinities of these metal adsorbates on diamond is provided in Table 4. The findings show that direct metal-carbon bonds tend to produce large NEA values but the different metal reactivities towards carbon greatly affect their properties. Metals that form carbides (*e.g.* Ti, V, Al) tend to be favoured, because a smaller M–C bond distance improves both the NEA and thermal stability of the surface layer. Conversely, metals such as Cu that do not form carbides, exhibit poor NEA, and in addition, will generally oxidise readily in ambient air or simply desorb at elevated temperatures.

Fogarty used DFT calculations to study a wide range of Ti structures on bare, oxygenated and nitrogenated diamond (100) surfaces [108]. For the bare surfaces, the titanium termination effectively creates a (sub)monolayer of titanium carbide (TiC) on the surface, with the titanium outermost. The Ti adopts a variety of linear or bridging geometries depending upon the coverage, as the surface reconstructs to minimise steric hindrance. The adsorption energies and EAs varied greatly depending on the TiC structure adopted. Table 4 shows data for two of the most promising TiC structures. The most stable TiC structure calculated was for a quarter monolayer (E_{ad} = −9.7 eV) which also had an NEA of −0.7 eV. The lowest EA was for a half-monolayer Ti coverage (−1.6 eV) – equalling that of the H-terminated surface – but with greater stability than the H-terminated surface. Both these TiC surfaces, therefore, are ideal candidates for further study, if methods can be found to obtain these specific surfaces experimentally.

Finite-temperature time-dependent DFT has been used to explore the thermionic behaviour of Li and H terminations [109]. Using an N-doped (100) diamond slab, a Richardson constant of 1.4 A cm^{-2} K^{-2} was obtained for Li-terminated diamond, higher than the value of 1 A cm^{-2} K^{-2} predicted for H-termination. Using predicted values for thermionic current in addition to work function and temperature, the maximum theoretical efficiency was determined to be 36% for a device operating at ~2500 K with a Li-

Table 4
Theoretical studies of maximum absorption energies, E_{ad}, and corresponding electron affinity (EA) of various metal adsorbates on the bare undoped diamond surface.

Termination	Surface	Coverage (ML)	E_{ad} (eV/atom)	Electron Affinity (eV)	Ref.
Li	(100)	1	−3.26	−2.70	[91]
Li	(111)	1	−1.50	−0.81	[116]
Ti	(100)	0.25	−4.71	−0.90	[117]
Ti	(100)	0.25	−9.70	−0.70	[106]
Ti	(100)	0.5	−7.80	−1.60	[106]
V	(100)	0.5	−6.60	−0.76	[115]
Ni	(100)	0.25	−4.25	−0.29	[115]
Cu	(100)	1	−2.93	−0.55	[115]
Al	(100)	1	−4.11	−1.47	[92]

terminated diamond emitter and H-terminated diamond collector. Despite the authors acknowledging this temperature is too high for practical use, this computational method nevertheless presents an interesting new approach to compare terminating species.

4.3.2. Metalloid terminations

Recently, experimental work at La Trobe University in Australia has shown that both Si [110,111] and Ge [112] exhibit small but stable NEA values (−0.86 eV and −0.71 eV, respectively) when directly bonded onto (100) diamond. Moreover, the Si adsorbate retained its NEA even when further oxidised, making it a very promising candidate for air-stable TEC devices [113], along with surface transfer doping applications [114]. However, no electron emission experiments have yet been published.

Although boron is commonly used to p-dope diamond, B also is slightly less electronegative than carbon (recall Fig. 10), such that a B-terminated diamond surface has the potential for NEA. A Chinese group recently reported the results of a theoretical study in which the NEA was calculated for B-termination on bare and oxygenated diamond (001) surfaces [93,115]. For 1-monolayer coverage, a B-terminated bare diamond (001) surface had an NEA of −1.39 eV, with corresponding adsorption energy of −6.85 eV per B atom. This energy is larger than that of a hydrogenated diamond (001) surface by 1.49 eV, suggesting that the B-terminated surface may be stable to temperatures suitable for thermionic emission. However, the stability of this surface to ambient air or oxidation has yet to be measured. The same group reported that B-termination onto an oxidised diamond showed a PEA of up to 3.21 eV.

Overall, there has been very little work reported, either experimentally or theoretically, on adsorbates onto bare diamond. Given the large number of possible adsorbates yet to be tested, this provides an excellent opportunity for future research.

4.3.3. Metal-oxygen terminations

Some of the problems associated with the metal-diamond system can be overcome by depositing the metal onto an already oxidised diamond surface [91]. While it may appear counterintuitive to surface terminate with electronegative O (EN = 3.5), provided a sufficiently electropositive metal is bonded on top of the oxygen layer, the overall combination can produce a net NEA. The surface charge distributions, however, are often complex and no longer resemble a simple dipole structure. Fig. 11 shows examples of the surface charge distribution (electrostatic potential) for three different diamond termination schemes calculated using DFT methods [118]. A structural overlay is included to show the relative positions of the bulk atoms and adsorbates within the slab structure. In each simulation the vacuum level is set to 0 eV. Within the bulk diamond there is a weakly modulated potential on top of an average well of depth ~14–16 eV, depending on the system. In contrast, the surface region exhibits a strongly oscillating potential that corresponds to the surface charge distribution induced by the adsorbates. In these plots, the curvature of the potential gives the charge density at that point. Therefore, using current sign convention, the peak regions correspond to higher local negative charge and the trough regions to higher positive charge. Thus, in Fig. 11(a) for hydrogenated diamond, there is a small dipole structure oriented perpendicular to the surface with the positive side (labelled 'A') situated on the H atoms facing the vacuum. For the Li–O-diamond case (Fig. 11(b)), a much larger dipole can be seen with the positive part located on the Li ('B') and the negative part ('C') now located between the C and O bonds. A more complex example is shown in Fig. 11(c) for the Na–O-diamond surface. Now there is a much more complicated charge distribution, with oscillating positive and negative regions, however there is still a large positive charge located outermost ('D'), which is necessary for NEA.

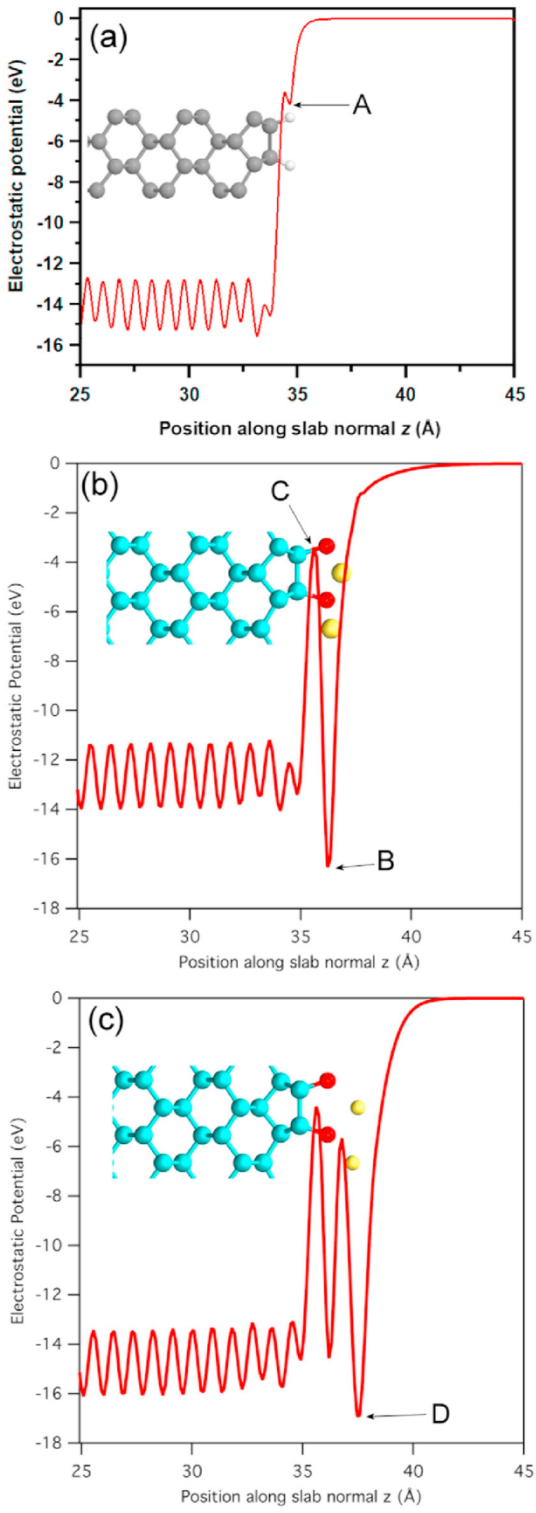

Fig. 11. DFT calculations of the plane-averaged electrostatic potential with a structural overlay to show the position of the diamond (100) surface atoms relative to the surface dipole features: (a) H-terminated diamond surface; (b) 1 monolayer of Li adsorbed onto an oxidised diamond surface; (c) 1 monolayer of Na adsorbed onto an oxidised diamond surface. Labels A-D show positions of interest discussed in the text. Plots (b) and (c) are adapted from O'Donnell *et al.* [116]. Copyright (2015) American Chemical Society.

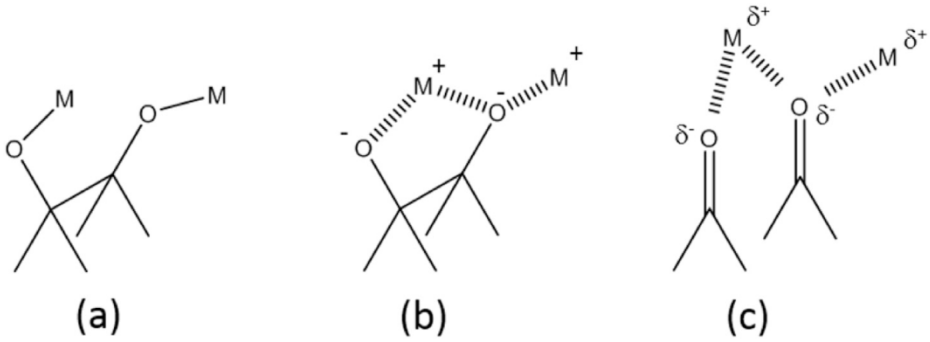

Fig. 12. Different possible interactions between a metal (M) and O-terminated diamond. (a) Covalent bond with oxygen, (b) ionic bond with oxygen and (c) dipolar interaction with oxygen. In each case, the metal can bond to a single O or bridge across two or more O atoms.

Metals can bond with O-terminated diamond surface in three different ways: covalent bonding, ionic bonding or a weaker dipolar interaction (Fig. 12). In each case, because the metal is effectively (partially) oxidised by being bonded to the oxygen on the surface, its reactivity toward further oxidation is reduced, making the surface more air-stable.

Practically, the M-O-diamond system adds another step for consideration because the oxygen-terminated surface is believed to be comprised of a mixture of different bonding arrangements, including ether (C_s—O—C_s, where C_s represents a surface carbon atom that is part of the diamond lattice), and ketone (C_s=O) configurations, and possibly also hydroxyl (C_s—OH) bonding, the relative proportions of which vary depending on the oxidation method used [119]. For covalent or ionically bonded O atoms, in order for the metal atom to attach, one of the existing C_s—O bonds first needs to break. This can be the π-bond of the ketone or a σ-bond of the ether, and may result in a surface reconstruction. The energetics of the multi-step metal adsorption process can thus become rather complex, but recent advances in computational surface modelling now allow these to be calculated with a reasonable degree of confidence. Table 5 gives details of computationally derived adsorption energies and electron affinities of various metal-O-diamond terminations.

4.3.4. Group I and II metals

One of the first metal-oxygen-diamond systems studied used caesium due to this metal being extremely electropositive. It was reported that CsO-termination possesses an air-stable NEA [122–124] capable of electron emission at low electric fields of 0.2 V μm^{-1} [125] but unfortunately it is not thermally stable above ~400 °C [121]. Computational work suggests that this is because the Cs—O interaction is a weak dipolar interaction, similar to that depicted in Fig. 12(c). A comparison of the Group I metals Li, Na, K and Rb, suggests that work function and NEA is not necessarily proportional to the electronegativity of the different metals, but lighter elements have a greatly enhanced thermal stability [91,116,126]. The reason for this is that the larger atoms tend to protrude from the surface due to steric crowding and so desorb at lower temperatures. Conversely, the smaller atoms are more tightly bound with near-ionic bonds (Fig. 12(b)), thus reside closer to the surface, and so are more resistant to desorption.

With these findings in mind, it is not surprising that the Li—O-diamond system has received significant attention. Initially, theoretical work [91,114] found Li—O-termination, consisting of up to 1 monolayer of Li on O-terminated diamond, possessed thermal stability similar to that of H-termination (~ −5 eV/atom). Importantly, the EA was predicted to be more negative than that of H-terminated diamond, up to −3.89 eV and −3.97 eV on (100) and (111) diamond, respectively.

Experimentally, two methods, the thick and thin film processes, have been used to achieve Li—O termination on (100) diamond, as shown in Fig. 13. In both cases, the diamond surface is first oxidised using a method such as plasma or ozone treatment. The thick-film process then involves deposition of 50–200 nm of Li onto the O-terminated diamond by evaporation or sputtering in vacuum [94,114]. The sample is usually then annealed at ~600 °C to react the Li with the O. Any excess (*i.e.* more than a monolayer) Li that does not react with O is chemically identical to bulk Li metal, and this can

Table 5
Theoretical studies of maximum absorption energies and corresponding electron affinities of various metal adsorbates on the oxygenated undoped diamond surface. For the larger metals, such as Al and Ti, multiple bonding geometries are possible depending upon surface coverage, and the adsorption energy and EA values can vary widely with the surface structure adopted. In these cases, only one example per report is given (usually the one with the lowest NEA), and the reader is directed to the associated reference for the others.

Termination	Surface	Coverage (ML)	E_{ad} (eV/atom)	EA (eV)	Ref.
Li	(100)	1	−3.64	−3.50	[116]
Li	(111)	0.5	−4.37	−3.97	[114]
Na	(100)	0.5	−2.41	−1.30	[116]
K	(100)	0.25	−2.44	−2.44	[116]
Cs	(100)	0.25	−2.19	−2.41	[116]
Mg	(100)	0.5	−3.92	−2.77	[116]
MgO	(111)	0.25	−5.27	−3.08	[120]
Al	(100)	0.25	−6.36	−0.37	[92]
Al	(111)	0.25	−7.31	−2.17	[118]
Ti	(100)	0.25	−7.60 – −7.80	−2.90 - −3.10	[106,121]
Ni	(100)	0.5	−3.80	−0.16	[119]
Cu	(100)	0.5	−2.35	−1.28	[119]
Zn	(100)	0.5	−1.13	−3.05	[119]

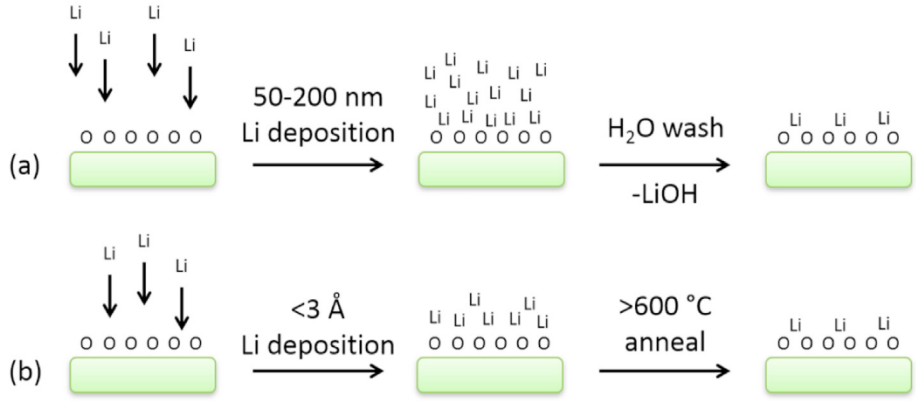

Fig. 13. Li deposition methods on O-terminated diamond. (a) Thick-film method where a thick Li layer is deposited, annealed, and the excess is removed by washing in water. (b) Thin-film method where a small amount of Li is deposited and excess (if any) is removed by annealing under UHV conditions.

be dissolved away by simply washing the sample in water. Although this method is quick and cheap, it proved to have poor reproducibility. The NEA was patchy across the surfaces, with some areas exhibiting large NEA values while others gave much lower values, or even had PEA. The reason for this poor reproducibility is not yet understood but it could be due a poorly controlled multi-bonded oxygen layer, that inhibits Li retention and co-ordination on the diamond surface.

By contrast, the thin-film process deposits a layer of Li < 3 Å thick using a UHV deposition technique, followed by the annealing step at >600 °C to 'activate' the NEA surface. Excess Li that is not chemically bonded to O desorbs from the surface at this temperature and is pumped away. Although more expensive and time-consuming, this thin-film method is reliable and controllable, and samples can be optimised by transferring them back and forth multiple times between a metal deposition chamber, an annealing chamber, and a characterisation chamber, all without breaking UHV. O'Donnell *et al.* [125] demonstrated NEA explicitly on Li–O-diamond by annealing at different temperatures, as shown in Fig. 14. The work function for the clean O-terminated diamond (PEA surface) was above 6 eV, and decreased as more Li was deposited. Each subsequent anneal at a higher temperature further lowered the work function while also increasing the emission intensity. Of particular interest is the 600 °C anneal which resulted in a sharp intensity increase, indicative of the transition from a PEA to a NEA surface, which was further supported by the double peak shown.

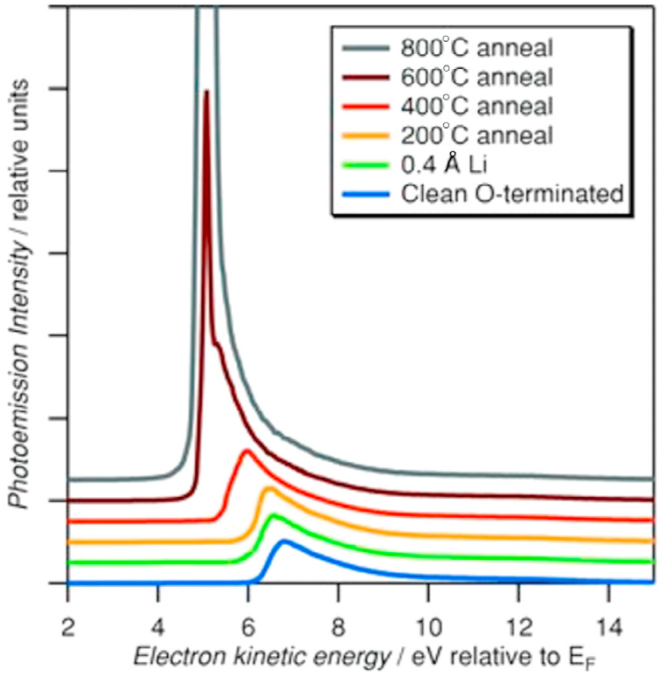

Fig. 14. Photoemission intensity from a lithiated diamond surface following different anneal temperatures. Reproduced with permission from Ref. [125]. Copyright (2013) Wiley-VCH Verlag GmbH & Co. KGaA, Weinheim.

Such lithiated surfaces show a 200 × secondary-electron-yield enhancement compared with a PEA surface [114,127]. The LiO-terminated surface exhibits true NEA as shown by total photoelectron yield spectroscopy, and is also confirmed to be air-stable, and thus does not undergo any surface transfer doping.

Insight into the behaviour of Group I metals on oxidised diamond surfaces was followed naturally by a study of magnesium. Theoretical calculations of Mg addition to O-terminated (100) diamond predicted similar adsorption energies and electron affinities to those of Li, but at only 0.5 monolayer (ML) coverage [116]. Subsequently, the Mg–O-terminated surface was shown experimentally to possess a large NEA of −2.0 eV with 1.5 Å Mg deposited using the thin-film method [128]. Unlike Li, no annealing step was required due to the greater reactivity to O of Mg than Li. This surface was confirmed to be both air and water stable, although the NEA diminished after air exposure but could be almost fully recovered after a vacuum anneal. This suggests the loss of NEA was due to temporary adsorption of atmospheric species such as water vapour.

Calculated surface geometries of the various Group I and II metals of Table 5 are shown in Fig. 15. For Li and Mg, the small metal atoms are located close to the surface, almost lying within the oxygen layer, and have a high surface coverage. Conversely, for larger atoms such as K and Cs, their larger size and steric hindrance leads to a lower surface density, and means that these atoms protrude some distance from the surface.

4.3.5. Transition metals

Nemanich and co-workers have conducted experimental studies of metal-O-diamond surface terminations utilising selected transition metals [99–101]. They report a measured NEA of −0.5 eV for thin (<10 Å) layers of Zr on oxidised (100) diamond, but no NEA was found for Co or Cu. Theoretical calculations by a group at Newcastle University of Ti, Ni, Cu and Zn on O-terminated (100) diamond showed that for monolayer and sub-monolayer coverages, PEA or NEA is often highly dependent on the nature of the

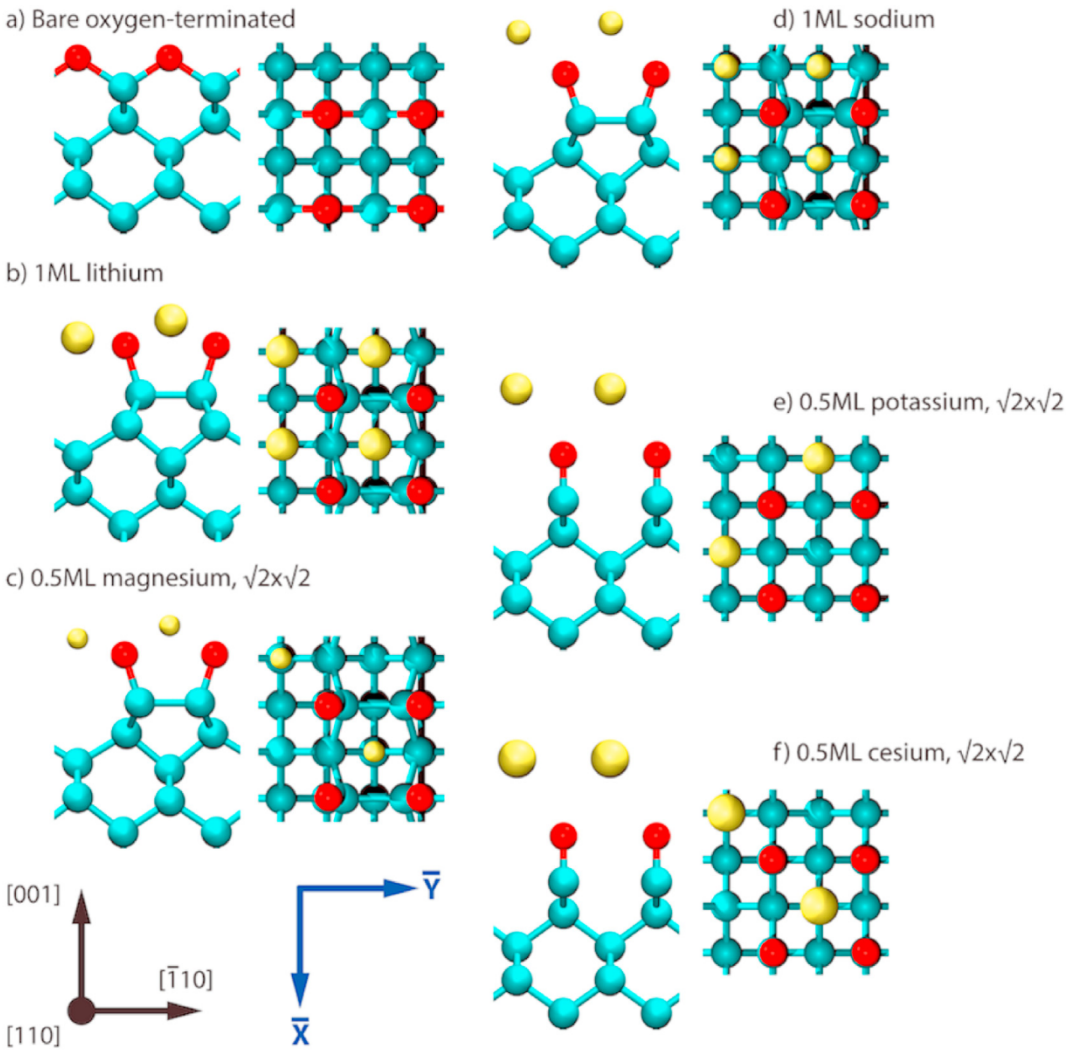

Fig. 15. Calculated locations of different Group I and II metal adsorbates in the metal-oxygen-diamond system. In each case, the side-view is on the left and plan-view on the right. Carbon is blue, oxygen is red, and the metal is yellow. ML = monolayer. Reprinted with permission from Ref. [116]. Copyright (2015) American Chemical Society. (A colour version of this figure can be viewed online.)

adsorption site [119,129]. Metal-O-diamond terminations involving transition metals have larger adsorption energies than those of Group I metals or H, which makes them promising candidates so long as a selective NEA surface is formed.

In another recent study, Cr and Ti were deposited on oxygen-terminated boron-doped diamond using the thick-film method, similar to the process shown in Fig. 13(a), although HCl was required to remove excess metal [130]. These metal oxides were stable up to the highest annealing temperature used, 650 °C. The TiO surface exhibited an effective NEA while the CrO surface exhibited a true NEA. This is consistent with the calculations of Fogarty [106] who predicted high stability and large NEA values for various TiO- coverages, especially in the quarter-monolayer case where one Ti atom bonds to 4 carbonyl carbons, as shown in Fig. 16.

4.3.6. Aluminium

The Al–O-diamond system has recently been studied computationally and experimentally on both the (100) and (111) diamond surfaces [50,92,118]. Computational work established that Al adsorption onto O-terminated diamond gave large adsorption energies on both (100) and (111) diamond at 0.25 ML Al coverage, due to the strong ionic bond that can form between Al and O. However, at larger coverages some Al–Al metallic bonding occurs, meaning that the Al is less ionic and so the surfaces generally exhibited PEA. Adsorption energies decreased with increasing Al coverage, which is desirable for avoiding island formation of the metal on the surface. Another study of different Al:O ratios on diamond also calculated NEA but determined only slightly favourable adsorption energy with respect to bulk Al_2O_3 [131].

Experimental work has determined an NEA up to −2.3 eV from Al deposition onto O-terminated diamond using the thick-film and thin-film methods [50]. For the thick-film method, HCl was required to remove excess metal. However, this surface was not determined to be thermally stable, with the work function varying with annealing temperature. This was not from Al desorbing from the surface, instead there was evidence to suggest Al could break both C–O bonds of the O-termination and form an aluminium oxide layer on the diamond surface. This represents a new issue for forming a metal-O-diamond surface termination that should be considered for similar elements.

4.3.7. Hydroxyl termination

Standard organic chemistry reactions have been widely used to functionalise the diamond surface, and present another potential

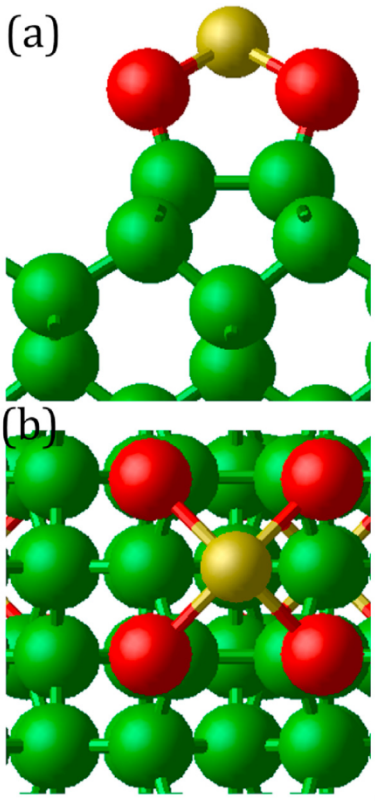

Fig. 16. Calculated geometry for a quarter-monolayer of Ti bonded to an oxygenated diamond (100) surface. (a) Side view, (b) top view. Green C, red = O, Yellow = Ti. Reprinted from Ref. [106] with permission. (A colour version of this figure can be viewed online.)

pathway to give the surface NEA. Hydroxyl (OH) termination can be viewed as a variant of the metal-O-diamond system but with hydrogen as the electropositive adsorbate. Different theoretical studies of hydroxyl-terminated diamond give varying predictions for the magnitude of the EA. Values of −0.6 eV [132], −0.55 eV [98], −2.13 eV [90] and −0.4 eV [72] have been calculated for OH on the (100) undoped diamond surface, and +0.3 eV on the (111) surface [72]. These values change significantly on n- or p-doped diamond surfaces [72]. For example, on B-doped (111) diamond there is a reasonable NEA of −0.9 eV, whereas for n-type diamond the EAs are large and positive, the largest being +4.3 eV for the P-doped (111) surface. The wide variation of values may be due to the difficulties of DFT to model hydrogen-bonding interactions. Hydroxyl termination has been formed experimentally *e.g.* by annealing hydrogenated (111) diamond surface at 500 °C in water vapour [133], but thus far no NEA has been demonstrated.

4.3.8. Nitrogen terminations (nitride, amine, ammonium and metal nitride)

Nitrogen can bond to the diamond surface in many different ways to satisfy its usual trivalency. These include primary amines (C_s–NH_2, where C_s represents a surface carbon), secondary-amines ($C_{s,1}C_{s,2}NH$) where the N bridges across 2 surface carbons, cyano groups (C_s–C≡N), and imino groups (–C_s=NH and –C_s=N–C_s). Thus, a 'nitrogenated' surface will always be composed of a mixture of these species, although the primary amine is usually by far the most prevalent due to its relative stability.

Theoretically, purely nitrogenated surfaces (*i.e.* those with no other elements apart from C and N present) have been calculated to have large PEA values of 3.2–4.7 eV [106] consistent with the experimental values [134,135], but with low stabilities.

Amine termination can be formed relatively easily from ammonia plasma treatment [136] or reaction of chlorinated diamond with ammonia or methylamine [137]. These surfaces can be protonated by immersion in aqueous HCl solution, to give predominantly surface ammonium (–NH_3^+) groups [138]. Zhu *et al.* demonstrated that both amine- and ammonia-terminated diamond surfaces exhibited NEA (although no values were reported) in vacuum and in water, and were capable of photocatalysis of N_2 into NH_3. However, no thermionic emission experiments on these surfaces have yet been reported. Theoretically, DFT calculation on the undoped diamond (100) and (111) surfaces gave NEA values of −0.8 and −0.7 eV, respectively, although these values changed significantly on doped diamond substrates [72]. Recent calculations by Fogarty [106] report EA values between −0.9 and −2.3 eV for NH_2 termination of (100) diamond for a range of bonding geometries and surface coverages.

An electropositive metal can bond to the nitrogenated diamond surface to form M-N-diamond surface structures. These are analogous to the MO-diamond structures discussed in section 4.3.3 and can have an overall net NEA provided the metal is sufficiently electropositive. One of the few examples reported to date is for Ti. Calculations show that the TiN-terminated surfaces are significantly more stable than the various amine structures, though there is little difference in the adsorption energies between the different coverage values or geometries adopted [106]. These surfaces exhibit EA values of between −1.7 eV and +1.8 eV, which is rather disappointing. Nevertheless, there are plenty of other metals that have yet to be tested in this metal-N-diamond termination scheme, and so these may yet hold out the prospect of finding a temperature-stable surface with extremely high NEA.

4.3.9. Cubic boron nitride

Recently a Chinese group has reported DFT calculations for monolayers of cubic boron nitride, with either the B or N layer outermost, on (111) diamond [139]. They investigated the effect of further terminating these NB or BN surfaces with H and F. The NBH- and NBF-terminated diamond both had positive EAs with no in-bandgap states. Indeed, the NBF-terminated diamond (111) surface was calculated to have the largest PEA (4.48 eV) reported for any diamond surface to date, exceeding the EAs of the N- and F-terminated diamond (111) surfaces by 2.53 eV and 1.95 eV, respectively. In contrast, the calculations predicted the BNH-terminated surface to have the largest NEA of any diamond surface (−4.0 eV) but unfortunately with an adsorption energy (−3.51 eV) lower than that for H on the (111) surface (recall Table 2). This means that thermionic emission applications are probably not really viable for this material, although it remains a highly promising candidate for low-temperature electron emission applications.

5. Conclusions

Diamond shows great promise for electron emission devices due to being able to form an NEA surface. Hydrogen termination is typically used in electron emission studies, but it is not air-stable and will desorb from the surface at elevated temperatures. By modifying the surface with the addition of monolayers or sub-monolayer coverage of metals or other electropositive adsorbates, different NEA surfaces can be formed. In particular, the metal-oxygen-diamond surface structure allows for high thermal stability, of interest for thermionic applications. Results to date suggest that small metal atom adsorbates are preferable to large ones, because they lie closer to the diamond surface and thus have high adsorption energies leading to increased temperature stability. Metals with high electropositivity, or which ionise easily to form

highly charged ions (Mg^{2+}, Al^{3+}, Ti^{4+}, Sc^{3+}), are good candidates for further investigation, as are Si and Ge which form strong, stable bonds with both carbon and oxygen. Boron termination on bare diamond has been predicted theoretically to be thermally stable and exhibit a reasonable NEA, however no experimental work has yet been reported for this system. The related termination approach using metal-N-diamond has only been reported for Ti, but calculations show that this, too, can exhibit NEA and high-temperature stability.

Combined with a suitable n-type dopant, these NEA surfaces may hold promise for future vacuum-based diamond-based thermionic power generation or waste-energy-scavenging applications. However, there are still unsolved problems with regard to mitigation of space-charge, overall power efficiency and optimal design of the TEC devices. The lack of supply of commercial large-area (3-inch or 4-inch diameter) diamond substrates is also a concern. At present, most diamond suppliers only sell substrates with areas ~10 × 10 mm, so unless the availability of larger area substrates increases rapidly this may be a limiting factor in the uptake of diamond TEC technology.

Along with thermionic applications, novel NEA surfaces are also being developed that are water-stable, for applications such as water splitting and photocatalysis [140]. NEA diamond surfaces with low work functions would also be extremely valuable for field-emission applications (ultra-fast radiation-hard electronics, bright wide-angle displays) and secondary-electron emission applications (night-vision goggles, portable X-ray sources). There are still many termination schemes that are yet to be tested, and so surface functionalisation of diamond represents a huge opportunity for future research.

CRediT author contribution statement

Michael C. James: Writing - original draft, Preparation, creation and/or presentation of the published work, specifically writing the initial draft. **Fabian Fogarty:** Writing - original draft, Preparation, creation and/or presentation of the published work, specifically writing the initial draft. **Ramiz Zulkharnay:** Writing - review & editing, Preparation, specifically critical review, commentary or revision — including pre-or postpublication stages. **Neil A. Fox:** Writing - review & editing, Preparation, specifically critical review, commentary or revision — including pre-or postpublication stages. **Paul W. May:** Writing - review & editing, Preparation, specifically critical review, commentary or revision — including pre-or post-publication stages.

Declaration of competing interest

The authors declare that they have no known competing financial interests or personal relationships that could have appeared to influence the work reported in this paper.

Acknowledgements

MCJ thanks the UK EPSRC for funding (EP/L016648/1) as part of the Functional Nanomaterials CDT. FF thanks the UK EPSRC for funding (EP/L015315/1) via the UK EPSRC Centre for Doctoral Training in Diamond Science and Technology. RZ wishes to thank the Bolashak International Scholarship programme (Republic of Kazakhstan) for funding support. PWM wishes to thank Neil Allan for useful discussions. No new data were created specifically for this review.

References

[1] A.T. Sowers, B.L. Ward, S.L. English, R.J. Nemanich, Field emission properties of nitrogen-doped diamond films, J. Appl. Phys. 86 (1999) 3973–3982.
[2] J.B. Cui, J. Ristein, M. Stammler, K. Janischowsky, G. Kleber, L. Ley, Hydrogen termination and electron emission from CVD diamond surfaces: a combined secondary electron emission, photoelectron emission microscopy, photoelectron yield, and field emission study, Diam. Relat. Mater. 9 (2000) 1143–1147.
[3] P.W. May, J.C. Stone, M.N.R. Ashfold, K.R. Hallam, W.N. Wang, N.A. Fox, The effect of diamond surface termination species upon field emission properties, Diam. Relat. Mater. 7 (1998) 671–676.
[4] M.W. Geis, J.C. Twichell, N.N. Efremow, K. Krohn, T.M. Lyszczarz, Comparison of electric field emission from nitrogen-doped, type Ib diamond, and boron-doped diamond, Appl. Phys. Lett. 68 (1996) 2294–2296.
[5] J.L. Van Noord, H. Kamhawi, H.K. Mcewen, Characterization of a high current, long life hollow cathode, 29th Int. Electr. Propuls. Conf. (2005). IEPC-2005-321, http://electricrocket.org/IEPC/321.pdf.
[6] J.L. Van Noord, NEXT ion thruster thermal model, *43rd AIAA/ASME/SAE/ASEE Jt*, Propuls. Conf. Exhib. (2007) 1–21.
[7] V.L. Granatstein, R.K. Parker, C.M. Armstrong, Scanning the technology - vacuum electronics at the dawn of the twenty-first century, Proc. IEEE 87 (1999) 702–716.
[8] P.J. Wilbur, R.G. Jahn, F.C. Curran, Space electric propulsion plasmas, IEEE Trans. Plasma Sci. 19 (1991) 1167–1179.
[9] K.P. Loh, I. Sakaguchi, M. Nishitani-Gamo, T. Taniguchi, T. Ando, Negative electron affinity of cubic boron nitride, Diam. Relat. Mater. 8 (1999) 781–784.
[10] R.J. Nemanich, P.K. Baumann, M.C. Benjamin, S.W. King, J. van der Weide, R.F. Davis, Negative electron affinity surfaces of aluminum nitride and diamond, Diam. Relat. Mater. 5 (1996) 790–796.
[11] O.W. Richardson, On the negative radiation from hot platinum, Proc. Camb. Philol. Soc. 11 (1901) 286–295.
[12] S. Dushman, Thermionic Emission, *Rev. Mod. Phys.* 2 (1930) 381–476.
[13] J.F. Morris, D.L. Jacobson, Thermionic Energy Conversion for Space-Power and Terrestrial-Topping Applications, IEEE, 1964, pp. 143–147.
[14] G.N. Hatsopoulos, J. Kaye, Measured thermal efficiencies of a diode configuration of a thermo electron engine, J. Appl. Phys. 29 (1958) 1124–1125.
[15] T.D. Musho, W.F. Paxton, J.L. Davidson, D.G. Walker, Quantum simulation of thermionic emission from diamond films, J. Vac. Sci. Technol. B 31 (2013), 021401.
[16] J. Voss, A. Vojvodic, S.H. Chou, R.T. Howe, I. Bargatin, F. Abild-Pedersen, Thermionic current densities from first principles, J. Chem. Phys. 138 (2013) 204701.
[17] R.O. Jenkins, A review of thermionic cathodes, Vacuum 19 (1969) 353–359.
[18] G. Xiao, G. Zheng, M. Qiu, Q. Li, D. Li, M. Ni, Thermionic energy conversion for concentrating solar power, Appl. Energy 208 (2017) 1318–1342.
[19] G.N. Hatsopoulos, E.P. Gyftopoulos, *Thermionic Energy Conversion: Processes and Devices*, MIT Press, Cambridge MA, 1973.
[20] S. Kimura, H. Yoshida, S. Uchida, A. Ogino, Surface electronic properties of Si-doped AlGaN and thermionic emission characteristics with adsorption of alkali metal atoms, Phys. Status Solidi 217 (2019) 1900719.
[21] C. Oshima, E. Bannai, T. Tanaka, S. Kawai, Thermionic work function of LaB_6 single crystals and their surfaces, J. Appl. Phys. 48 (1977) 3925–3927.
[22] H. Liu, X. Zhang, S. Ning, Y. Xiao, J. Zhang, The electronic structure and work functions of single crystal LaB_6 typical crystal surfaces, Vacuum 143 (2017) 245–250.
[23] K. Togawa, T. Shintake, T. Inagaki, K. Onoe, T. Tanaka, H. Baba, H. Matsumoto, CeB_6 electron gun for low-emittance Injector, Phys. Rev. Spec. Top. Accel. Beams 10 (2007), 020703.
[24] H. Liu, X. Zhang, Y. Xiao, J. Zhang, The electronic structure and thermionic emisson property of single crystal SmB_6 typical crystal surfaces, Vacuum 145 (2017) 295–298.
[25] X. Yang, et al., High temperature performance of coaxial h-BN/CNT wires above 1,000 °C: thermionic electron emission and thermally activated conductivity, Nano Res. 12 (2019) 1855–1861.
[26] K.A.A. Khalid, T.J. Leong, K. Mohamed, Review on thermionic energy converters, IEEE Trans. Electron. Dev. 63 (2016) 2231–2241.
[27] P. Shefsiek, Describing and correlating the performance of the thermionic converter: a historical perspective, IEEE Trans. Plasma Sci. 38 (2010) 2041–2047.
[28] J.M. Houston, Theoretical efficiency of the thermionic energy converter, J. Appl. Phys. 30 (1959) 481–487.
[29] P.G. Tanner, D.A. Fraser, A.D. Irving, Developments in thermionic energy converters, IEE Proc. Sci. Meas. Technol. 152 (2005) 1–6.
[30] F.A.M. Koeck, R.J. Nemanich, Advances in thermionic energy conversion through single-crystal n-type diamond, Front. Mech. Eng. 3 (2017) 1–11.
[31] E.J.W. Smith, et al., Mixed-size diamond seeding for low-thermal-barrier growth of CVD diamond onto GaN and AlN, Carbon 167 (2020) 620–626.
[32] O. Dunseath, et al., Studies of black diamond as an antibacterial surface for gram negative bacteria: the interplay between chemical and mechanical bactericidal activity, Sci. Rep. 9 (2019) 8815.
[33] M. Islam, O.T. Inal, J.R. Luke, Development of electron reflection suppression materials for improved thermionic energy converter performance using thin

film deposition techniques, J. Appl. Phys. 100 (2006), 084903.
[34] F.A.M. Koeck, R.J. Nemanich, J. Sharp, Doped diamond thin film electron sources for thermionic energy conversion, 26th Int. Vac. Nanoelectron. Conf. IVNC (2013) 1–3, 2013.
[35] W.F. Paxton, S. Ravipati, M.M. Brooks, M. Howell, J.L. Davidson, Thermionic emission from diamond films in molecular hydrogen environments, Front. Mech. Eng. 3 (2017).
[36] F.A.M. Koeck, R.J. Nemanich, Y. Balasubramaniam, K. Haenen, J. Sharp, Enhanced thermionic energy conversion and thermionic emission from doped diamond films through methane exposure, Diam. Relat. Mater. 20 (2011) 1229–1233.
[37] J.H. Lee, I. Bargatin, N.A. Melosh, R.T. Howe, Optimal emitter-collector gap for thermionic energy converters, Appl. Phys. Lett. 100 (2012) 173904.
[38] F.A.M. Koeck, R.J. Nemanich, Emission characterization from nitrogen-doped diamond with respect to energy conversion, Diam. Relat. Mater. 15 (2006) 217–220.
[39] B.Y. Moyzhes, T.H. Geballe, The thermionic energy converter as a topping cycle for more efficient heat engines — new triode designs with a longitudinal magnetic field, J. Phys. D Appl. Phys. 38 (2005) 782–786.
[40] S. Meir, C. Stephanos, T.H. Geballe, J. Mannhart, Highly-efficient thermoelectronic conversion of solar energy and heat into electric power, J. Renew. Sustain. Energy 5 (2013), 043127.
[41] R. Wanke, G.W.J. Hassink, C. Stephanos, I. Rastegar, W. Braun, J. Mannhart, Magnetic-field-free thermoelectronic power conversion based on graphene and related two-dimensional materials, J. Appl. Phys. 119 244507.
[42] I. Bickerton, N.A. Fox, Improving the efficiency of a thermionic energy converter using dual electric fields and electron beaming, Front. Mech. Eng. 3 (2017) 14.
[43] A. Croot, G. Wan, A. Rowan, H.D. Andrade, J.A. Smith, N.A. Fox, Beta-radiation enhanced thermionic emission from diamond thin films, Front. Mech. Eng. 3 (2017) 1–8.
[44] W.P. Kang, J.L. Davidson, A. Wisitsora-at, Y.M. Wong, R. Takalkar, K. Holmes, D.V. Kerns, Diamond vacuum field emission devices, Diam. Relat. Mater. 13 (2004) 1944–1948.
[45] C.A. Spindt, A thin-film field-emission cathode, J. Appl. Phys. 39 (1968) 3504–3505.
[46] R.L. Harniman, O.J.L. Fox, W. Janssen, S. Drijkoningen, K. Haenen, P.W. May, Direct observation of electron emission from grain boundaries in CVD diamond by PeakForce-controlled tunnelling atomic force microscopy, Carbon 94 (2015) 386–395.
[47] R. Harniman, P.W. May, O.J.L. Fox, Direct observation of electron emission from CVD diamond grain boundaries by tunnelling atomic force microscopy Independent of surface morphology, Diam. Relat. Mater. 80 (2017) 147–152.
[48] V.S. Robinson, Y. Show, G.M. Swain, R.G. Reifenberger, T.S. Fisher, Thermionic emission from surface-terminated nanocrystalline diamond, Diam. Relat. Mater. 15 (2006) 1601–1608.
[49] K. Uppireddi, T.L. Westover, T.S. Fisher, B. Weiner, G. Morell, Thermionic emission energy distribution from nanocrystalline diamond films for direct thermal-electrical energy conversion applications, J. Appl. Phys. 106 (2009), 043716.
[50] M.C. James, *Aluminium And Oxygen Termination Of Diamond for Thermionic Applications*, PhD Thesis, University of Bristol, UK, 2019.
[51] A.W. Raja, P. Zilio, A. Alabastri, R.P. Zaccaria, J. Cunha, Photon-Enhanced Thermionic Emission, ESA, 2015. Available online, https://pdfs.semanticscholar.org/af2f/6b015de4b729d85b3e4936a00e4cbdf84023.pdf.
[52] M. Kataoka, C. Zhu, F.A.M. Koeck, R.J. Nemanich, Thermionic electron emission from nitrogen-doped homoepitaxial diamond, Diam. Relat. Mater. 19 (2010) 110–113.
[53] F.A.M. Koeck, R.J. Nemanich, A. Lazea, K. Haenen, Thermionic electron emission from low work-function phosphorus doped diamond films, Diam. Relat. Mater. 18 (2009) 789–791.
[54] D.V. Paramonov, M.S. El-Genk, A review of cesium thermionic converters with developed emitter surfaces, Energy Convers. Manag. 38 (1997) 533–549.
[55] A. Kribus, G. Segev, Solar energy conversion with photon enhanced thermionic emission, J. Optic. 18 (2016), 073001.
[56] S. Elfimchev, M. Chandran, R. Akhvlediani, A. Hoffman, Trap-assisted photon-enhanced thermionic emission from polycrystalline diamond films, Phys. Status Solidi 212 (2015) 2583–2588.
[57] T. Sun, F.A.M. Koeck, C. Zhu, R.J. Nemanich, Combined visible light photoemission and low temperature thermionic emission from nitrogen doped diamond films, Appl. Phys. Lett. 99 (2011) 202101.
[58] N. Neugebohrn, T. Sun, F.A.M. Koeck, G.G. Hembree, R.J. Nemanich, T. Schmidt, J. Falta, Spatial correlation of photo-induced and thermionic electron emission from low work function diamond films, Diam. Relat. Mater. 40 (2013) 12–16.
[59] A. Bellucci, P. Calvani, M. Girolami, D.M. Trucchi, Defect engineering of diamond cathodes for high temperature solar cells, *2015*, IEEE 15th Int. Conf. Environ. Electr. Eng. - Conf. Proc. (2015) 1616–1619.
[60] A. Bellucci, P. Calvani, M. Girolami, S. Orlando, R. Polini, D.M. Trucchi, Optimization of black diamond films for solar energy conversion, Appl. Surf. Sci. 380 (2016) 8–11.
[61] P. Calvani, A. Bellucci, M. Girolami, S. Orlando, V. Valentini, R. Polini, D.M. Trucchi, Black diamond for solar energy conversion, Carbon 105 (2016) 401–407.
[62] M. Girolami, L. Criante, F. Di Fonzo, S. Lo Turco, A. Mezzetti, A. Notargiacomo, M. Pea, A. Bellucci, P. Calvani, V. Valentini, D.M. Trucchi, Graphite distributed electrodes for diamond-based photon-enhanced thermionic emission solar cells, Carbon 111 (2017) 48–53.
[63] South West Nuclear Hub, The diamond battery, Available online at: https://southwestnuclearhub.ac.uk/research/case-studies/diamond-battery/.
[64] C. Delfaure, M. Pomorski, J. de Sanoit, P. Bergonzo, S. Saada, Single crystal CVD diamond membranes for betavoltaic cells, Appl. Phys. Lett. 108 (2016) 252105.
[65] V.S. Bormashov, et al., High power density nuclear battery proto-type based on diamond Schottky diodes, Diam. Relat. Mater. 84 (2018) 41–47.
[66] J. Gubbi, R. Buyya, S. Marusic, M. Palaniswami, Internet of Things (IoT): a vision, architectural elements, and future directions, Future Generat. Comput. Syst. 29 (2013) 1645–1660.
[67] P.W. May, Diamond thin films: a 21st-century material, Phil. Trans. Roy. Soc. Lond. 358 (2000) 473–495.
[68] P.W. May, W.J. Ludlow, M. Hannaway, P.J. Heard, J.A. Smith, K.N. Rosser, Raman and conductivity studies of boron-doped microcrystalline diamond, facetted nanocrystalline diamond and cauliflower diamond films, Diam. Relat. Mater. 17 (2008) 105–117.
[69] M.N.R. Ashfold, J.P. Goss, B.L. Green, P.W. May, M.E. Newton, C.V. Peaker, Nitrogen in diamond, Chem. Rev. 120 (2020) 5745–5794.
[70] S. Koizumi, *n-Type diamond Growth and the semiconducting properties*, Ch.2.2, in: S. Koizumi, H. Umezawa, J. Pernot, M. Suzuki (Eds.), Power Electronics Device Applications of Diamond Semiconductors, Woodhead Publishing, Duxford, UK, 2018.
[71] C. Nebel, J. Ristein (Eds.), *Thin-Film Diamond I*: (Part of the *Semiconductors And Semimetals Series*, vol. 76, Academic Press, 2003.
[72] K. Larsson, The combined influence of dopant species and surface termination on the electronic properties of diamond surfaces, J. Carbon Res. 6 (2020) 22.
[73] J. Raymakers, K. Haenen, W. Maes, Diamond surface functionalization: from gemstone to photoelectrochemical applications, J. Mater. Chem. C 7 (2019) 10134–10165.
[74] D. Zhu, L. Zhang, R.E. Ruther, R.J. Hamers, Photo-illuminated diamond as a solid-state source of solvated electrons in water for nitrogen reduction, Nat. Mater. 12 (2013) 836–841.
[75] J.S. Lapington, V. Taillandier, B.L. Cann, J. Howorth, J. Milnes, R. Vaz, P.W. May, N.A. Fox, R. Stevens, L. Wang, Investigation of the secondary electron emission characteristics of alternative dynode materials for imaging photomultipliers, J. Instrum. 7 (2012) E04002, an Erratum to: J. Instrum. **7** (2012) C03018.
[76] F. Maier, J. Ristein, L. Ley, Electron affinity of plasma-hydrogenated and chemically oxidized diamond (100) surfaces, Phys. Rev. B 64 (2001) 165411.
[77] J.B. Cui, J. Ristein, L. Ley, Electron affinity of the bare and hydrogen covered single crystal diamond (111) surface, Phys. Rev. Lett. 81 (1998) 429–432.
[78] K. Kimura, K. Nakajima, S. Yamanaka, M. Hasegawa, H. Okushi, Hydrogen analysis of CVD homoepitaxial diamond films by high-resolution elastic recoil detection, Nucl. Instrum. Methods Phys. Res. B 190 (2002) 689–692.
[79] H. Kawarada, Hydrogen-terminated diamond surface and interface, Surf. Sci. Rep. 26 (1996) 205–259.
[80] F.A.M. Koeck, R.J. Nemanich, Substrate-diamond interface considerations for enhanced thermionic electron emission from nitrogen doped diamond films, J. Appl. Phys. 112 (2012) 113707.
[81] F.A.M. Koeck, R.J. Nemanich, Sulfur doped nanocrystalline diamond films as field enhancement based thermionic emitters and their role in energy conversion, Diamond Relat. Mater. 14 (2005) 2051–2054.
[82] M. Suzuki, T. Ono, N. Sakuma, T. Sakai, Low-temperature thermionic emission from nitrogen-doped nanocrystalline diamond films on n-type Si grown by MPCVD, Diamond Relat. Mater. 18 (2009) 1274–1277.
[83] W.F. Paxton, T. Wade, M. Howell, N. Tolk, W.P. Kang, J.L. Davidson, Thermionic emission characterization of boron-doped microcrystalline diamond films at elevated temperatures, Phys. Status Solidi 209 (2012) 1993–1995.
[84] F.A.M. Koeck, R.J. Nemanich, Low temperature onset for thermionic emitters based on nitrogen incorporated UNCD films, Diam. Relat. Mater. 18 (2009) 232–234.
[85] P. Strobel, M. Riedel, J. Ristein, L. Ley, Surface transfer doping of diamond, Diam. Relat. Mater. 430 (2004) 439–441.
[86] W.F. Paxton, M. Howell, W.P. Kang, J.L. Davidson, Influence of hydrogen on the thermionic electron emission from nitrogen-Incorporated polycrystalline diamond films, J. Vac. Sci. Technol. B 30 (2012), 021202.
[87] W.F. Paxton, A. Steigerwald, M. Howell, N. Tolk, W.P. Kang, J.L. Davidson, The effect of hydrogen desorption kinetics on thermionic emission from polycrystalline chemical vapor deposited diamond, Appl. Phys. Lett. 101 (2012).
[88] J. Van Der Weide, Z. Zhang, P.K. Baumann, M.G. Wensell, J. Bernholc, R.J. Nemanich, Negative-Electron-affinity effects on the diamond (100) surface, Phys. Rev. B 50 (1994) 5803–5806.
[89] J. Furthmüller, J. Hafner, G. Kresse, Surface reconstruction and electronic properties of clean and hydrogenated diamond (111) surfaces, Phys. Rev. B 53 (1996) 7334–7351.
[90] M.J. Rutter, J. Robertson, *Ab initio* calculation of electron affinities of diamond surfaces, Phys. Rev. B 57 (1998) 9241–9245.
[91] K.M. O'Donnell, T.L. Martin, N.A. Fox, D. Cherns, *Ab initio* investigation of lithium on the diamond C(100) surface, Phys. Rev. B 82 (2010) 115303.
[92] M.C. James, A. Croot, P.W. May, N.L. Allan, Negative electron affinity from

aluminium on the diamond (100) surface: a theoretical study, J. Phys. Condens. Matter 30 (2018) 235002.
[93] W. Shen, Y. Pan, S. Shen, H. Li, Y. Zhang, G. Zhang, Electron affinity of boron-terminated diamond (001) surfaces: a density functional theory study, J. Mater. Chem. C 7 (2019) 9756–9765.
[94] T.L. Martin, Lithium Oxygen Termination as a Negative Electron Affinity Surface on Diamond: a Computational and Photoemission Study, PhD Thesis, University of Bristol, UK, 2011.
[95] H. Kato, D. Takeuchi, M. Ogura, T. Yamada, M. Kataoka, Y. Kimura, S. Sobue, C.E. Nebel, S. Yamasaki, Heavily phosphorus-doped nano-crystalline diamond electrode for thermionic emission application, Diam. Relat. Mater. 63 (2016) 165–168.
[96] T. Sun, F.A.M. Koeck, P.B. Stepanov, R.J. Nemanich, Interface and interlayer barrier effects on photo-induced electron emission from low work function diamond films, Diam. Relat. Mater. 44 (2014) 123–128.
[97] R.T. Longo, Physics of thermionic dispenser cathode aging, J. Appl. Phys. 94 (2003) 6966–6975.
[98] H. Dominguez-Andrade, J. Anaya, A. Croot, M. Cattelan, D.J. Twitchen, M. Kuball, N.A. Fox, Correlating thermionic emission with specific surface reconstructions in a <100> hydrogenated single-crystal diamond, ACS Appl. Mater. Interfaces 12 (2020) 26534–26542.
[99] W.M. Haynes, CRC Handbook of Chemistry and Physics, 96th ed., CRC Press, Boca Raton, 2015.
[100] S.J. Sque, R. Jones, P.R. Briddon, Structure, electronics, and interaction of hydrogen and oxygen on diamond surfaces, Phys. Rev. B 73 (2006), 085313.
[101] P.K. Baumann, R.J. Nemanich, Characterization of copper-diamond (100), (111), and (100) interfaces: electron affinity and Schottky barrier, Phys. Rev. B 58 (1998) 1643–1654.
[102] P.K. Baumann, R.J. Nemanich, Characterization of cobalt-diamond (100) interfaces: electron affinity and Schottky barrier, Appl. Surf. Sci **104-**105 (1996) 267–273.
[103] P.K. Baumann, R.J. Nemanich, Electron emission from metal-diamond (100), (111) and (110) interfaces, Diamond Relat. Mater. 7 (1998) 612–619.
[104] J. van der Weide, R.J. Nemanich, Influence of Interfacial hydrogen and oxygen on the Schottky barrier height of nickel on (111) and (100) diamond surfaces, Phys. Rev. B 49 (1994) 13629–13637.
[105] J. van der Weide, R.J. Nemanich, Schottky barrier height and negative electron affinity of titanium on (111) diamond, J. Vac. Sci. Technol. B 10 (1992) 1940–1943.
[106] F.A.M. Köck, J.M. Garguilo, B. Brown, R.J. Nemanich, Enhanced low-temperature thermionic field emission from surface-treated N-doped diamond films, Diam. Relat. Mater. 11 (2002) 774–779.
[107] F.A.M. Koeck, J.M. Garguilo, R.J. Nemanich, On the thermionic emission from nitrogen-doped diamond films with respect to energy conversion, Diam. Relat. Mater. 13 (2004) 2052–2055.
[108] F. Fogarty, Renewable Energy – Low Temperature Thermionic Emission from Modified Diamond Surfaces, PhD Thesis, University of Bristol, UK, 2020.
[109] T. Shinozaki, S. Hagiwara, N. Morioka, Y. Kimura, K. Watanabe, Real-time first-principles simulations of thermionic emission from N-doped diamond surfaces, Appl. Phys. Express 11 (2018), 064301.
[110] A. Schenk, A. Tadich, M. Sear, K.M. O'Donnell, L. Ley, A. Stacey, C. Pakes, formation of a silicon terminated (100) diamond surface, Appl. Phys. Lett. 106 (2015) 191603.
[111] A.K. Schenk, A. Tadich, M.J. Sear, D. Qi, A.T.S. Wee, A. Stacey, C.I. Pakes, The surface electronic structure of silicon terminated (100) diamond, Nanotechnology 27 (2016) 275201.
[112] M.J. Sear, A.K. Schenk, A. Tadich, B.J. Spencer, C.A. Wright, A. Stacey, C.I. Pakes, Germanium terminated (100) diamond, J. Phys. Condens. Matter 29 (2017) 145002.
[113] A.K. Schenk, M.J. Sear, A. Tadich, A. Stacey, C.I. Pakes, Oxidation of the silicon terminated (100) diamond surface, J. Phys. Condens. Matter 29 (2017), 025003.
[114] M.J. Sear, A.K. Schenk, A. Tadich, A. Stacey, C.I. Pakes, P-type surface transfer doping of oxidised silicon terminated (100) diamond, Appl. Phys. Lett. 110 (2017), 011605.
[115] Z. Sun, M. Yang, X. Wang, P. Wang, C. Zhang, N. Gao, H. Li, Boron-terminated diamond (100) surfaces with promising structural and electronic properties, Phys. Chem. Chem. Phys. 22 (2020) 8060–8066.
[116] K.M. O'Donnell, T.L. Martin, M.T. Edmonds, A. Tadich, L. Thomsen, J. Ristein, C.I. Pakes, N.A. Fox, L. Ley, Photoelectron emission from lithiated diamond, Phys. Status Solidi 211 (2014) 2209–2222.
[117] A.K. Tiwari, J.P. Goss, P.R. Briddon, N.G. Wright, A.B. Horsfall, M.J. Rayson, Electronic and structural properties of diamond (001) surfaces terminated by selected transition metals, Phys. Rev. B 86 (2012) 155301.
[118] K.M. O'Donnell, T.L. Martin, N.L. Allan, Light metals on oxygen-terminated diamond (100): structure and electronic properties, Chem. Mater. 27 (2015) 1306–1315.
[119] J. Navas, et al., Oxygen termination of homoepitaxial diamond surface by ozone and chemical methods: an experimental and theoretical perspective, Appl. Surf. Sci. 433 (2018) 408–418.
[120] M.C. James, P.W. May, N.L. Allan, *Ab initio* study of negative electron affinity from light metals on the oxygen-terminated diamond (111) surface, J. Phys. Condens. Matter 31 (2019) 295002.
[121] A.K. Tiwari, J.P. Goss, P.R. Briddon, A.B. Horsfall, N.G. Wright, R. Jones, M.J. Rayson, Unexpected change in the electron affinity of diamond caused by the ultra-thin transition metal oxide films, Europhys. Lett. 108 (2014) 46005.
[122] W.E. Pickett, Negative electron affinity and low work function surface: cesium on oxygenated diamond (100), Phys. Rev. Lett. 73 (1994) 1664–1667.
[123] K.P. Loh, J.S. Foord, R.G. Egdell, R.B. Jackman, Tuning the electron affinity of CVD diamond with adsorbed caesium and oxygen layers, Diam. Relat. Mater. 5 (1997) 874–878.
[124] L. Diederich, O.M. Kuttel, P. Aebi, E. Maillard-Schaller, R. Fasel, L. Schlapbach, Photoelectron emission from the negative electron affinity caesiated natural diamond (100) surface, Diam. Relat. Mater. 7 (1998) 660–665.
[125] M.W. Geis, J.C. Twichell, J. Macaulay, K. Okano, Electron field emission from diamond and other carbon materials after H_2, O_2, and Cs treatment, Appl. Phys. Lett. 67 (1995) 1328–1330.
[126] J.L. Nie, H.Y. Xiao, X.T. Zu, First principles calculations on Na and K-adsorbed diamond (100) surface, Chem. Phys. 326 (2006) 308–314.
[127] K.M. O'Donnell, M.T. Edmonds, J. Ristein, A. Tadich, L. Thomsen, Q.-H. Wu, C.I. Pakes, L. Ley, Diamond surfaces with air-stable negative electron affinity and giant electron yield enhancement, Adv. Funct. Mater. 23 (2013) 5608–5614.
[128] K.M. O'Donnell, M.T. Edmonds, A. Tadich, L. Thomsen, A. Stacey, A. Schenk, C.I. Pakes, L. Ley, Extremely high negative electron affinity of diamond via magnesium adsorption, Phys. Rev. B 92 (2015), 035303.
[129] A.K. Tiwari, J.P. Goss, P.R. Briddon, N.G. Wright, A.B. Horsfall, M.J. Rayson, Effect of different surface coverages of transition metals on the electronic and structural properties of diamond, Phys. Status Solidi 209 (2012) 1697–1702.
[130] M.Z. Othman, Studies Of N-type Doping And Suface Modification Of CVD Diamond for Use in Thermionic Applications, PhD Thesis, University of Bristol, UK, 2014.
[131] J.M.A. Beattie, J.P. Goss, M.J. Rayson, P.R. Briddon, Electron-affinity and surface-stability of aluminium-oxide terminated diamond surfaces, Diam. Relat. Mater. 94 (2019) 137–145.
[132] M. Kaviani, P. Deák, B. Aradi, T. Frauenheim, J.P. Chou, A. Gali, Proper surface termination for luminescent near-surface NV centers in diamond, Nano Lett. 14 (2014) 4772–4777.
[133] R. Yoshida, D. Miyata, T. Makino, S. Yamasaki, T. Matsumoto, T. Inokuma, N. Tokuda, formation of atomically flat hydroxyl-terminated diamond (111) surfaces via water vapor annealing, Appl. Surf. Sci. 458 (2018) 222–225.
[134] A. Stacey, et al., Nitrogen terminated diamond, Adv. Mater. Interfaces 2 (2015) 1500079.
[135] J.P. Chou, A. Retzker, A. Gali, Nitrogen-terminated diamond (111) surface for room-temperature quantum sensing and simulation, Nano Lett. 17 (2017) 2294–2298.
[136] J.J. Wei, J.L. Liu, L.X. Chen, L.F. Hei, F.X. Lv, ChM. Li, Amination of diamond film by ammonia microwave plasma treatment, Diam. Relat. Mater. 54 (2015), 43-38.
[137] J.B. Miller, Amines and thiols on diamond surfaces, Surf. Sci. 439 (1999) 21–33.
[138] D. Zhu, J.A. Bandy, S. Li, R.J. Hamers, Amino-terminated diamond surfaces: photoelectron emission and photocatalytic properties, Surf. Sci. 650 (2016) 295–301.
[139] W. Shen, S. Shen, S. Liu, H. Li, Z. Gan, Q. Zhang, Monolayer cubic boron nitride terminated diamond (111) surfaces for quantum sensing and electron emission applications, ACS Appl. Mater. Interfaces 12 (2020) 33336–33345.
[140] R.J. Hamers, J.A. Bandy, D. Zhua, L. Zhang, Photoemission from diamond films and substrates into water: dynamics of solvated electrons and Implications for diamond photoelectrochemistry, Faraday Discuss 172 (2014) 397–411.